

EVALUATING ATMOSPHERIC CORRECTION METHODS USING ASTER IMAGE

PEARSON BANDA

Thyolo, Malawi

Dissertation submitted to Ndata School of Climate and Earth Sciences of the Malawi University of Science and Technology in partial fulfilment of the requirements for the Bachelor of Science degree in Geo- Information and Earth Observation Sciences

July, 2021

DISSERTATION APPROVED BY:

SUPERVISOR:

Mr. I.R. Emmanuel Chinkaka Signature: _____

ASSESSOR:

Mr. S. Gondwe Signature: _____

Dr. C. Chisenga Signature: _____

DISCLAIMER

This document describes work undertaken as part of a programme of study at Ndata School of Climate and Earth Sciences of the Malawi University of Science and Technology. All views and opinions expressed therein remain the sole responsibility of the author, and do not necessarily represent those of the school.

COPYRIGHT STATEMENT:

This copy of the dissertation has been supplied on condition that anyone who consults it is understood to recognize that its copyright rests with its author and that no quotation from the dissertation and no information derived from it may be published without acknowledgement.

ABSTRACT

This research presents an evaluation of two atmospheric correction (AC) methods applied to ASTER image. The aim of this study was to determine the most suitable atmospheric correction method for ASTER satellite images by evaluating different methods of AC. The ASTER images used in this research were acquired in October 2004, over Kangankunde, an area with rare earth elements deposit found in Balaka district of Malawi. The study also used laboratory USGS ASTER resampled spectral reflectance library data.

In this research, FLAASH and Log residual AC methods were applied to ASTER image. The results of the AC methods were compared separately with each other. Then the comparisons were done with laboratory USGS ASTER resampled spectral reflectance library data. Lastly, band ratio technique was used to map different mineral groups at the study area.

From the results, FLAASH AC method was found to be a better AC method for mineral exploration and mapping. The log residual method, appeared to miss some specific absorption features as it could generalize much in terms of reflectance. Each of the AC methods did show some unknown features at different wavelengths which are recommended for further investigation. Mineral maps produced by band ratio techniques showed some small differences in mineral abundances as well as, spatial distributions. The comparisons were affected by unavailability of some datasets such as field data to show correlation between the image corrected data and field data through scatterplots. We expect this research to contribute its value to the understanding of potential issues and sources of errors in processes of AC and image analysis techniques and the selection of suitable AC method for aster image. Overall, we found that the FLAASH method is a better AC method than the log residual method.

ACKNOWLEDGEMENTS

First and foremost, praises and thanks to Jesus Christ, who is the God, the Almighty, for His showers of blessings throughout my research work to complete the research successfully.

I would like to express my gratitude to my supervisor Emmanuel Chinkaka for his, guidance, support, and suggestions. I really feel indebted for his contributions to this study and also for his willingness to help in every moment, challenging questions, and invaluable guidance in writing of this thesis.

I am also very grateful to all my lecturers for their provided mentoring that broadened my knowledge. I would especially like to thank Mr. N.S. Ngalonde for his willingness and support throughout my studies.

Finally, I would like to thank my loved ones. My greatest thanks to my mom and dad [James and Patricia Banda; Patsen and Thokozani Chirwa] for their love, prayers, caring, sacrifices and financial support throughout my study. Many thanks to my fiancée Mphatso Kaunda for her support, patience and love. Thanks to my sisters, brothers and all friends especially Innocent Banda for his help, motivation and encouragements. I'm also very grateful to my pastor, Hanrick Matthews Phiri for his prayers throughout my study.

TABLE OF CONTENTS

1. Introduction 1
1.1. Background Statement 1
1.2. Problem statement 1
1.2. Main Objective 2
1.2.1. Specific Objectives 2
1.3. Research Questions 2
1.4. Significance of the Study 3
2. Literature Review 3
3. Methodology 6
3.1. Research design 6
3.2. Materials and methods 8
3.2.1. Study Site 8
3.2.2. Satellite data 11
3.2.3. Weather conditions 12
3.2.4. Auxiliary data 14
3.2.5. Radiative transfer model based atmospheric corrections 14
3.2.6. FLAASH-The Fast Line-of-sight Atmospheric Analysis of Spectral Hypercubes 16
3.2.7. Log Residuals 22
4. Results and Discussion 27
4.1.1. FLAASH and Log residual corrected images 27
4.1.2. Comparison of atmospheric correction results with ASTER USGS resampled library data 29
5.1.1. Mineral mapping results 33
5.1.1.1. Band ratio results 33
5.2. Discussion 39

5.2.1. Comparisons of atmospheric correction results with library data 39

5.2.2. Mineral mapping results 40

References 42

Appendices 46

ACRONYMS/ABBREVIATIONS

Cases

AC: Atmospheric Correction 6
ASTER: Advanced spaceborne Thermal Emission and Reflection Radiometer 5
DOS: Dark Object Subtraction 4
EL: Emperical Line 4
ENVI: Environment for Visualizing images 18
FF: Flat Field 4
FLAASH: The Fast Line-of-sight Atmospheric Analysis of Spectral Hypercubes 2, 17
REE: Rare Earth Elements 9
RTM: Radiative Transfer model 4
SWIR: Shortwave Infrared 8
VNIR: Visible to Near Infrarred 8

LIST OF FIGURES

Figure 1. Flow chart 7

Figure 2. Geological map of the Kangankunde carbonatite complex showing sample locations (after Broom-Fendley et al. (2017) Inset shows the location of Kangankunde in Malawi, Africa. 9

Figure 3. Field photographs of carbonatite outcrops at Kangankunde (Chikanda et. al., 2019). 10

Figure 4. An example of reflectance and radiance spectra. A- radiance spectrum of non-vegetated area and B- the surface reflectance spectrum after atmospheric correction (Clark et al., 2002). 15

Figure 5. Showing statistical results before and after applying post FLAASH processing equation..... 21

Figure 6. Classification of the Kangankunde carbonatites using molar proportions of CaO, MgO, and FeO + MnO (after Grittins and Harmer). Arrows indicate the trends that occur with increasing contents of the specified minerals. 25

Figure 7. Showing spectrum for unprocessed Aster data from one ROI image data. 27

Figure 8. FLAASH and Log residual corrected image spectra of different sites. 28

Figure 9. Comparison between library spectra and FLAASH corrected image spectra. 29

Figure 10. Comparison between resampled ASTER library spectra and Log residual corrected image spectra for the two sites P1 and P2. 30

Figure 11. Spectral comparison between Log residual, FLAASH and the resampled ASTER library spectra of two different sites P1 and P2. 31

Figure 12. Differences of the surface reflectance estimated by FLAASH (FLA) and Log residual (Log) and USGS ASTER resampled library spectra data. Positive values show overestimation and negative values show underestimation of the reflectance compared to the library data. 32

Figure 13. Band ratio mineral group maps for Log residual. 35

Figure 14. Band ratio mineral group maps for FLAASH. 36

Figure 15. RGB maps for Log residual and FLAASH produced from Mg-OH, Fe-OH and Al-OH band ratios. 38

LIST OF TABLES

Table 1. ASTER satellite image band specifications (ASTER USERS Handbook, 2005). 12

Table 2. Weather conditions in Balaka, Malawi on the dates of ASTER image acquisition. The data source is Weather Spark (2021) 14

Table 3. The input parameters used in FLAASH for the ASTER image. 20

Table 4. ASTER bands and band ratios by Rowan 26

Table 5. Spectral similarity results between AC corrected image spectra and library spectra using SFF and SAM methods. 33

1. Introduction

1.1. Background Statement

Remote sensing science is characterized by the evaluation and examination of data obtained from indirect physical interaction with the materials or objects (Levin, 1999). In this study, remote sensing denotes the use of satellite or aircraft-based sensor technologies to detect and classify objects on Earth. Rocks and minerals reflect and absorb electromagnetic radiation as a function of the wavelength of the radiation. Reflectance spectra show these variations in reflection and absorption for various wavelengths. By studying the reflectance spectra of rocks, individual minerals and groups of minerals may be identified. The region between 0.4µm to 2.5µm is mostly used in remote sensing to identify different groups of minerals as each group has a characteristic reflection spectrum, for example phyllo-silicates, carbonates, sulphates, and iron oxides and hydroxides (Clark, 1999). In optical remote sensing image analysis, converting at sensor radiance values into reliable surface reflectance data is a key for identifying and mapping of mineral composition of the surface. Radiance measured at sensor represents only relative brightness values of the target surface due to effects of the Earth's atmosphere, sun illumination, topography, etc. (Gupta, 2018).

1.2. Problem statement

Remote sensing data has proved to be an effective source of information for mineral mapping, land cover monitoring as well as lithological discrimination of the geological units. However, the nature of remote sensing requires that solar radiation pass through the atmosphere before it is collected by the instrument. Because of this, remotely sensed images include information about the atmosphere and the earth's surface. For those interested in quantitative analysis of surface reflectance, removing the influence of the atmosphere is a critical pre-processing step. To compensate for atmospheric effects, properties such as the amount of water vapor, distribution of aerosols, and scene visibility must be known (Levin, 1999). Because direct measurements of these atmospheric properties are rarely available, there are techniques that are used to remove their influence on multispectral or

hyperspectral radiance data. These properties are then used to constrain highly accurate models of atmospheric radiation transfer to produce an estimate of the true surface reflectance.

At present, common atmospheric correction methods can be roughly divided into the following; the statistical method, the pixel correlation model method, and the radiative transfer model method. The first method considers only the image data itself that do not require the actual ground spectral and environmental parameters measurements theoretically. This study, will focus on comparing two atmospheric correction techniques under statistical methods which are the Fast Line-of-sight Atmospheric Analysis of Spectral Hypercubes (FLAASH) technique and Log residuals technique.

1.2. Main Objective

To derive the most suitable AC method for ASTER imagery data by comparing FLAASH and Log residual AC methods

1.2.1. Specific Objectives

i. To investigate the effect of the different AC method on the derived reflectance spectra
ii. To compare the differences in the derived spectra for each AC method with the laboratory USGS ASTER resampled spectral reflectance library data
iii. To Evaluate differences in the mineral group maps produced from the output of AC methods

1.3. Research Questions

i. What is the most suitable AC method based on the reflectance spectra?
ii. Which spectral region has the most variations in absorption features of reflectance spectra derived from each AC method?
iii. How much do mineral mapping results change due to different AC methods

1.4. Significance of the Study

Atmospherically corrected surface reflectance data is important for many aspects: 1. the shapes of reflectance spectra are indications of chemical and physical properties of the surface materials; 2. reflectance data can be analyzed for quantitative change detection evaluation (Clark, 2002). Spectral shape caused by poor atmospheric correction may be interpreted as a false anomaly, and its investigation could lead to a waste of time and money (Clark, 2002). Therefore, well-calibrated reflectance data has greater validity and confidence in providing realistic surface properties and consequently result in accurate surface compositional maps.

2. Literature Review

Since the early 1960s, the scope of remote sensing has expanded in terms of its application to geological mapping and mineral exploration. At first, remote sensing was employed as a quick and cost-effective way to analyze spatial variations in lithology (Kerr et al., 2011). During the 1970s, geologists employed remote sensing techniques using airborne systems (Rowan & Mars, 2003). Improvement in spectral resolution in the modern-day remote sensing techniques has greatly improved the ability to distinguish different mineral types and rock groups (Clark, 1999). A wide variety of minerals such as carbonates, clays, and hydroxides can be sensed through this method (Clark et al., 2007). A lot of scholars showed the capability of the remote sensing approaches to identify and map minerals and rocks based on its particular spectra which are significant for exploring the mineral deposits (Mars & Rowan, 2011).

The ranges between 0.45 to 2.5 μm of the reflectance spectra are considered an essential part of the spectrum for geo-remote sensing applications. These ranges can be used in determining the composition of minerals on the basis of absorption characteristics (Neave et al., 2016). Carbonatites that are enriched with about fifty percent or more of calcite minerals display a strong absorption feature of the CO_3^{2-} ion, which is recognized easily within the range of 2.2- 2.33 μm (Kokaly, 2011). The iron minerals and REE elements, which may find in Ferro-carbonatite in abundance, also impact reflectance spectra. The iron absorption characteristics exhibit a distinctive absorption and are pronounced within

the window of 0.9-1.3 μm (Clark et al., 2007). REE absorption features are linked to electronic transitions in Nd^{3+}, which generates absorption characteristics in the wavelength ranges between 0.5 and 0.8 um (ENVI, 2014). A blend of these absorption features could yield a basis for the creation of carbonatite maps using remote-sensing data. The reflection spectra properties of carbonatites have previously been applied to prior investigations to produce maps of carbonatite complexes using aircraft sensors.

The aim of atmospheric correction is to retrieve the surface reflectance from the remotely sensed imagery by removing the effects of the atmospheric particles that absorb or scatter electromagnetic radiation reflected by different features on the earth surface (Clark et al., 2002). Generally, approaches for atmospheric corrections can be divided into two main groups: empirical methods and model-based methods. Earlier studies include several empirical methods, such as dark object subtraction (DOS), empirical line (EL) calibration, flat field (FF) calibration method and internal average relative reflectance (IARR) (Gao, 2009). These empirical methods are scene-based, except EL, which requires in-site reflectance measurements of bright and dark target areas in the site. In addition, empirical methods provide only relative surface reflectance while Radiative Transfer Models (RTM) based methods perform absolute calibration of remote sensing image with higher accuracy (Gupta, 2018). RTM methods are based on complex theoretical modelling of the atmospheric absorption and scattering by water vapor, aerosols and gases and, thus they require data on atmospheric conditions at the time of image acquisition (Kale, 2017). Ben-Dor. (2004), state that users tend to move to RTM methods because it provides reasonable results and does not require a field visit. Radiative transfer models named as LOWTRAN, MODTRAN, HITRAN, 5S and 6S are all reference models (Tempfli, 2009) and they are used for basic calculations in atmospheric correction software packages. Some of the software packages are: ATREM (Gao & Davis, 1997) and HATCH (Qu, 2003) are developed based on 5S and 6S models, while ATCOR (Richter & Schläpfer, 2002), ACORN (Miller, 2002) and FLAASH (Perkins, 2012) and Log residuals are based on MODTRAN models. Absolute atmospheric correction is more preferable than the relative correction

techniques (Nikolakopoulos et. al., 2002) as it models the atmosphere according to the similar environmental and geographical conditions when the image is acquired.

Advance Spaceborne Thermal Emission and Reflection Radiometer (ASTER) satellite sensor is one of the five state of the art instrumental sensor systems on-board Terra a satellite launched on December 18, 1999 at Vandenberg Air Force Base, California, USA. It is a multispectral sensor that flies at an altitude of about 705 km in a sun-synchronous orbit with a temporal resolution of 16 days. The swath width for all the ASTER sensors is 60km (Abrahams & Ramachandran). ASTER utilizes a unique combination of wide spectral coverage and high spatial resolution in the visible near-infrared through shortwave infrared to the thermal infrared regions (ASTER USERS Handbook, 2005). It is a partnership between NASA, Japan's Ministry of Economy, Trade and Industry (METI), the National Institute of Advanced Industrial Science and Technology (AIST) in Japan, and Japan Space systems. The ASTER sensor is capable of detecting more bands than previous sensors such as LANDSAT5, which allows geologists to map rocks and minerals on the surface of the earth with more accuracy. ASTER data contributes to a wide array of global change related application areas including geology and soil, vegetation and ecosystem dynamics, hydrology, and land cover change.

The ASTER instruments acquire data in three native spatial resolutions:

- VNIR (Visible and Near-Infrared) Bands 1, 2, 3N, 3B at 15m spatial resolution
- SWIR (Shortwave Infrared) Bands 4 - 9 at 30m spatial resolution
- TIR (Thermal Infrared) Bands 10 – 14 at 90m spatial resolution

Band 3 nadir (3N) and band 3 backward-looking (3B) allows capability of creating a Digital Elevation Model when both bands are acquired.

This research focused on evaluating two RTM atmospheric correction methods on ASTER data captured at Kangankunde, one of the largest hydrothermal alteration system deposit in the Chilwa Alkaline complex, located in Balaka, Malawi.

3. Methodology

3.1. Research design

This research involved evaluating two different atmospheric correction (AC) methods to determine the best AC method for ASTER data. FLAASH and log residual AC methods were applied to ASTER satellite images. The image was acquired on 22 October 2004. The FLAASH method was performed with rural aerosol model, then both methods outputs were compared with the library spectral data. Finally, for the mineral mapping, band ratio technique was used. Below is a summarized flow chart that shows the main steps where these methods were carried out. Main steps carried out in the research are illustrated by dashed lines. The datasets used in the study are highlighted by light blue color. The following subsections will describe each of the used methods in detail. The figure 1 below show the flowchart of the processes involved.

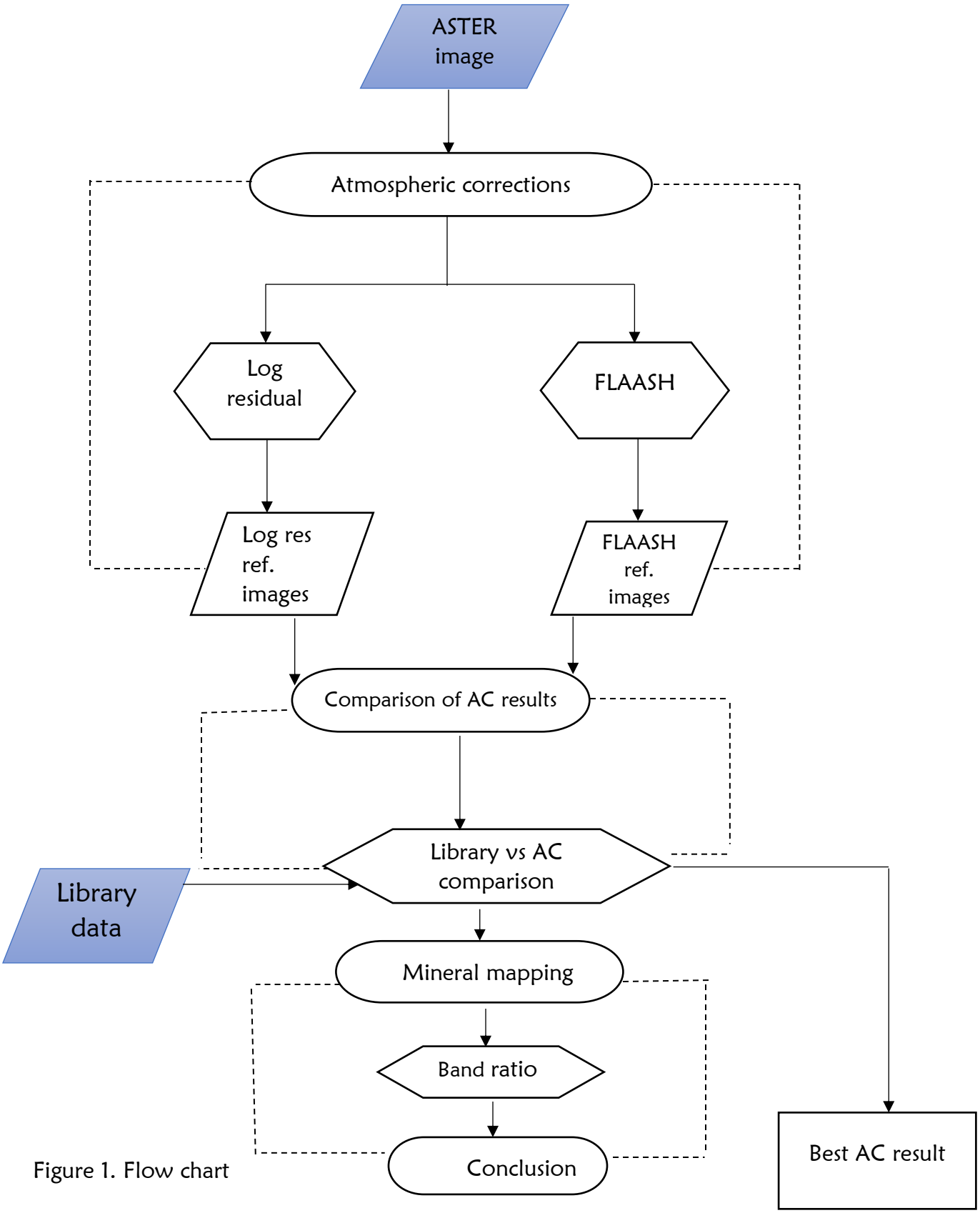


Figure 1. Flow chart

3.2. Materials and methods

3.2.1. Study Site

Kangankunde is located 100km North of Blantyre and 25km from the Nacala rail corridor. The place is chosen as a study area based on several reasons: 1. the area hosts hydrothermal mineral groups consisting of VNIR and SWIR active minerals; 2. data availability which can be easily downloaded from USGS website; 3. the area has scarce vegetation hence appropriate for geological remote sensing studies.

The Kangankunde Carbonatite Complex is one of the largest REE deposits in the Chilwa Alkaline. The complex has been a target for mineral exploration due to its amenable REE Minerals concentrations hence a detailed description of the complex is given in previous studies (Chikanda et. Al., 2019). The Lower Cretaceous Kangankunde complex is aligned N–S parallel to rift valley faults a few kilometers to the west of the East African Rift System. The complex consists of the main complex and a northern and southern knoll. There is a distinct zonation with regards to the lithologies of the main complex. The central core lithology which consists of carbonatite agglomerate is cut by carbonatite dykes and surrounded by a ring of feldspathic breccia and agglomerate. The first intrusion stage comprises apatite–dolomite characteristics and followed by the intrusion of dolomitic to ferroan–dolomitic carbonatite. The Kangankunde Carbonatite Complex is similar to other carbonatites in that it comprises a carbonatite body surrounded by a fenite aureole. The figure 2 below shows a detailed geologic map of the area created by Broom-Fendley et al (2017).

Geological map of the Kangankunde Carbonatite complex

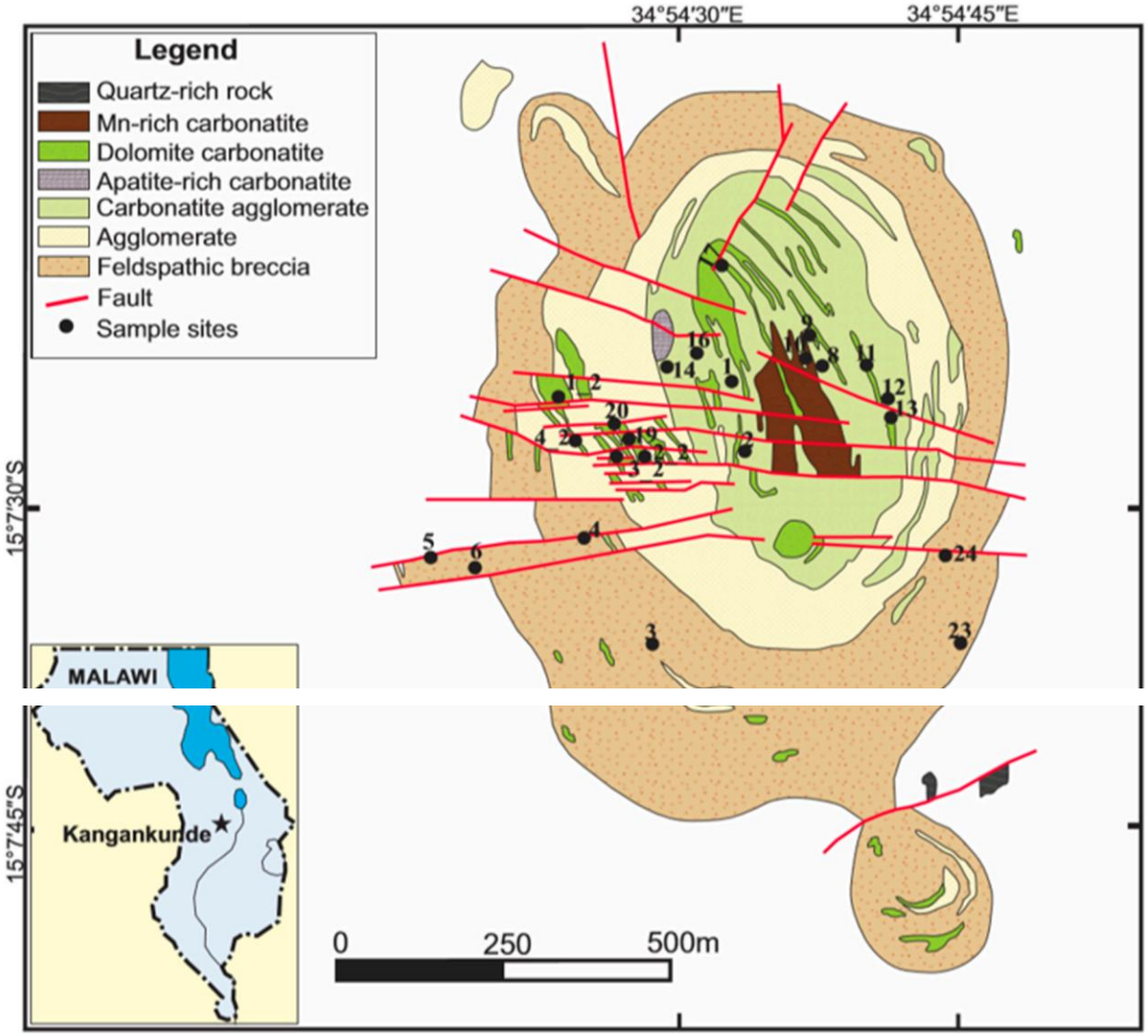


Figure 2. Geological map of the Kangankunde carbonatite complex showing sample locations (after Broom-Fendley et al. (2017) Inset shows the location of Kangankunde in Malawi, Africa.

The main geological units of the Kangankunde Carbonatite Complex comprise Mn- and REE-rich carbonatites, dolomite carbonatites, apatite-rich carbonatites, carbonatite agglomerate, quartz-rich rocks, and a fenite aureole that surrounds the main carbonatite body. The REE-rich carbonatites are concentrated in the center of the complex, with others

occurring irregularly in veins and dykes (commonly as dolomitic and ankeritic carbonatites) that intrude different units of the carbonatite body. Throughout the complex, outcrops of carbonatite are commonly cut by veins that formed from late (carbothermal) intrusions.

Faults occur both regionally and locally in some of the carbonatites of the Chilwa Alkaline Complex. These faults are different from the local faults that developed at Kangankunde, which commonly strike NW and are absent in other carbonatite bodies in the Chilwa Alkaline Province. Well-developed monazite veins of a few cm in width are ubiquitous in the Kangankunde complex and cut carbonatite and fenite breccias. Carbonatite agglomerates with distinct bulbous textures that resulted from weathering of the carbonate were observed in some lithologies.

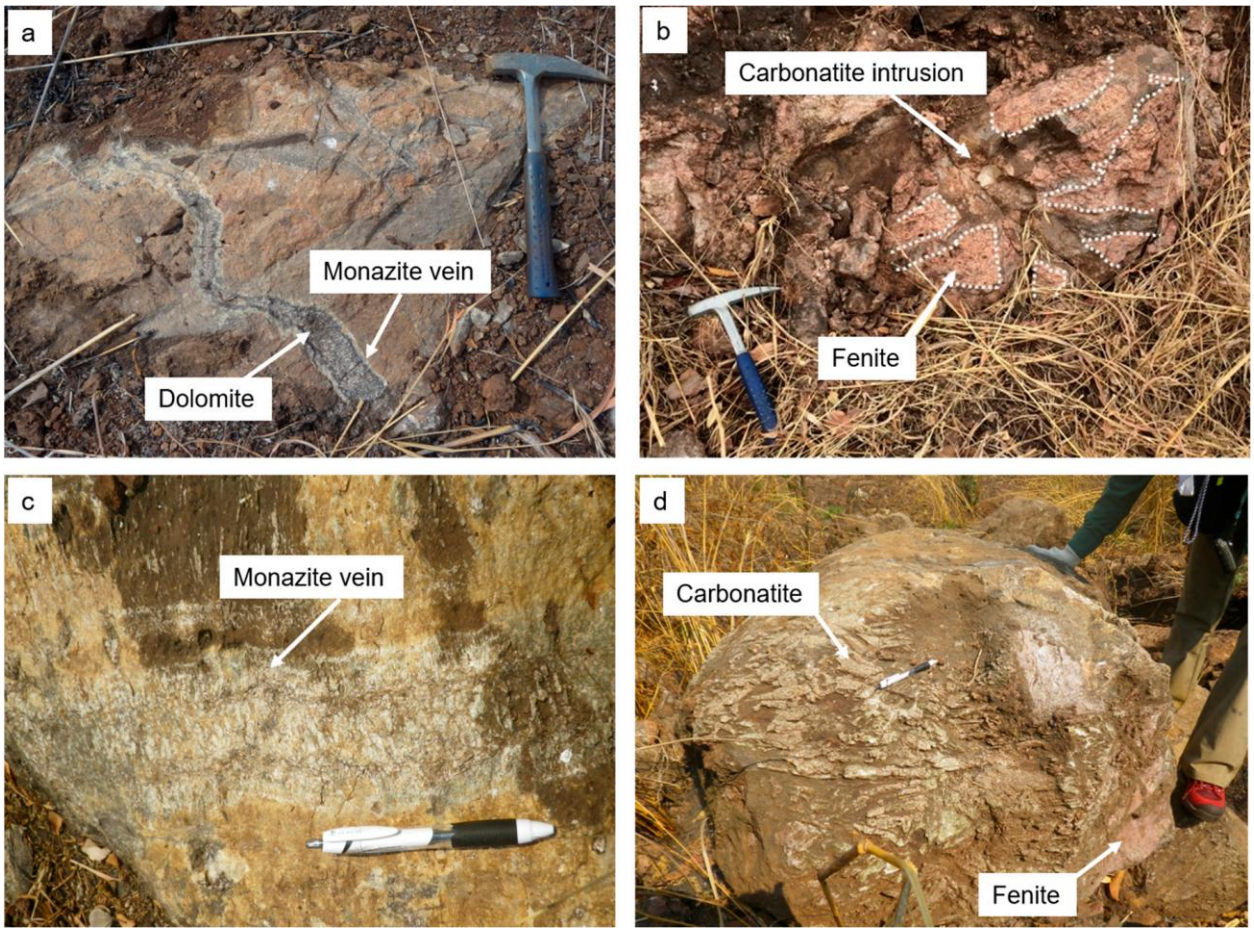


Figure 3. Field photographs of carbonatite outcrops at Kangankunde (Chikanda et. al., 2019).

3.2.2. Satellite data

The datasets used in this research were ASTER satellite image data acquired in October 2004. This data was collected when ASTER sensor was functioning well hence there was no need for crosstalk correction.

The ASTER image used is a L1T orthorectified image, the coordinate system of which is UTM projection zone 36S with WGS 84 datum. The dataset includes a multispectral image with 3 bands in VNIR, a multispectral image with 6 bands in SWIR regions and another multispectral image with 5 bands in TIR region. For this study, we used only VNIR and SWIR bands because these are the regions in which the alteration minerals have specific absorption features, VNIR bands were resampled to 30m from 15m so that we should not lose spatial details in SWIR bands if we reduced their spatial resolution. Table 1 below summarizes the ASTER spectral bands details.

Table 1. ASTER satellite image band specifications (ASTER USERS Handbook, 2005).

Subsystem	Band No.	Spectral Range (μm)	Spatial Resolution (m)	Quantization Levels
VNIR	1	0.52-0.60	15	8 bits
	2	0.63-0.69		
	3N	0.78-0.86		
	3B	0.78-0.86		
SWIR	4	1.60-1.70	30	8 bits
	5	2.145-2.185		
	6	2.185-2.225		
	7	2.235-2.285		
	8	2.295-2.365		
	9	2.360-2.430		
TIR	10	8.125-8.475	90	12 bits
	11	8.475-8.825		
	12	8.925-9.275		
	13	10.25-10.95		
	14	10.95-11.65		

3.2.3. Weather conditions

RTM based atmospheric correction methods require data on atmospheric conditions when the image is acquired. According to the information collected in Balaka, Malawi from January 1, 1990 to December 31, 2016, Balaka weather conditions can be summarized as below.

Temperature

In Balaka, the wet season is muggy and overcast, the dry season is mostly clear, and it is warm year-round. Over the course of the year, the temperature typically varies from 15°C to 32°C and is rarely below 14°C or above 35.5°C.

The hot season lasts for 2.2 months, from September 25 to November 30, with an average daily high temperature above 30.6°C. The hottest day of the year is November 1, with an average high of 31.7°C and low of 22.8°C.

The cool season lasts for 2.4 months, from May 28 to August 8, with an average daily high temperature below 26°C. The coldest day of the year is July 10, with an average low of 15.6°C and high of 24°C.

Clouds

In Balaka, the average percentage of the sky covered by clouds experiences extreme seasonal variation over the course of the year. The clearer part of the year in Balaka begins around March 31 and lasts for 7.5 months, ending around November 14. On June 25, the clearest day of the year, the sky is clear, mostly clear, or partly cloudy 92% of the time, and overcast or mostly cloudy 8% of the time. The cloudier part of the year begins around November 14 and lasts for 4.5 months, ending around March 31. On January 14, the cloudiest day of the year, the sky is overcast or mostly cloudy 83% of the time, and clear, mostly clear, or partly cloudy 17% of the time.

Rainfall

The average sliding 31-day rainfall during October in Balaka is rapidly increasing, starting the month at 0.3 inches, when it rarely exceeds 0.8 inches or falls below -0.0 inches, and ending the month at 1.7 inches, when it rarely exceeds 4.0 inches or falls below 0.2 inches.

Wind

The wind experienced at any given location is highly dependent on local topography and other factors, and instantaneous wind speed and direction vary more widely than hourly averages. The average hourly wind speed in Balaka is essentially constant during October, remaining within 0.1 miles per hour of 9.4 miles per hour throughout.

For reference, on October 13, the windiest day of the year, the daily average wind speed is 9.5 miles per hour, while on January 31, the calmest day of the year, the daily average

wind speed is 5.5 miles per hour. The highest daily average wind speed during October is 9.5 miles per hour on October 13.

Table 2. Weather conditions in Balaka, Malawi on the dates of ASTER image acquisition. The data source is Weather Spark (2021)

Time	Temperature (°C)	Wind (mph)	Humidity (%)	Visibility (km)	Clouds
6:00	**20**	**19.31**	**5%**	**40**	**clear**
9:00	23	12.88	10%	40	clear
12:00	25	9.65	7%	40	clear
15:00	27	10.46	3%	40	clear
18:00	22	12.26	9%	30	partly

3.2.4. Auxiliary data

In this research, apart from the satellite data, the geological map of Kangankunde (Broom-Fendley et al, 2017) and weather condition data obtained from Weather Spark were used.

3.2.5. Radiative transfer model based atmospheric corrections

Atmospheric correction of the ASTER image was carried out using two different radiative transfer models (RTM) based methods which are FLAASH and Log residuals. RTM based atmospheric correction methods involves simulating the relationship between the atmospheric parameters of the satellite synchronization and the true reflectivity of the surface by simulating the radiation transmission process between the atmospheric-surface remote sensor (Liang & Wang, 2010). Atmospheric modelling includes correction for absorption by atmospheric gases (H_2O at 0.94, 1.14, 1.38, 1.88μm; CO_2 at 2.01, 2.08μm, O_2 at 0.76μm; and O_3, N_2O, CO, CH_4, NO_2 at various wavelengths) over the range 0.4-2.5μm and scattering by atmospheric gaseous molecules (Rayleigh scattering in 0.4-0.7μm) and aerosols (Gao et al., 2009). Figure below illustrates how a radiance image

spectrum is converted to a surface reflectance spectrum after applying an atmospheric correction.

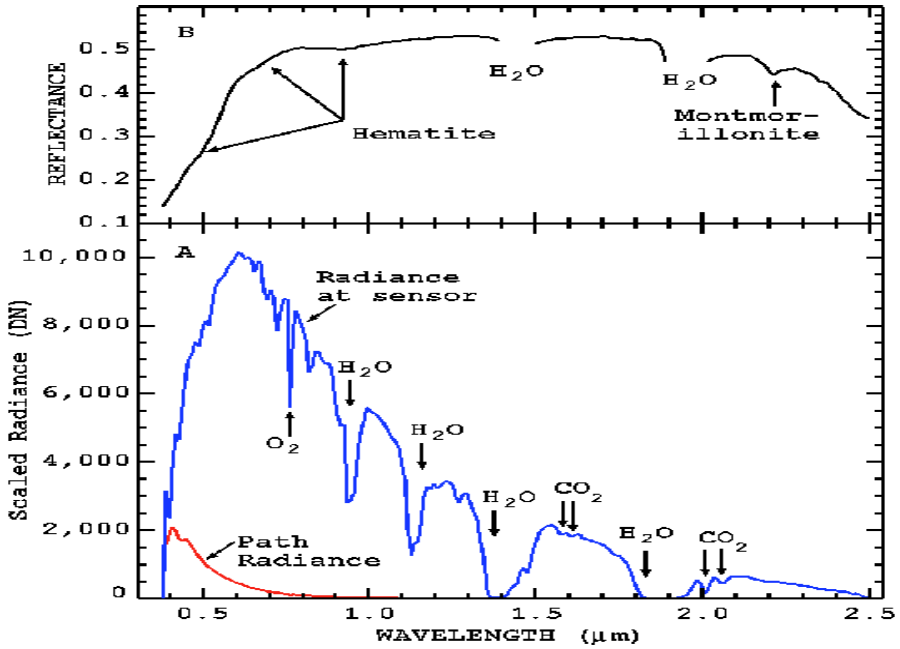


Figure 4. An example of reflectance and radiance spectra. A- radiance spectrum of non-vegetated area and B- the surface reflectance spectrum after atmospheric correction (Clark et al., 2002).

In this figure (A)- a radiance spectrum of the non-vegetated area has a strong influence of solar illumination and absorptions by atmospheric gases. (B)- After atmospheric correction, the spectrum shows absorption features of the minerals (hematite and montmorillonite) on the surface. The water features in the spectrum A are caused by atmospheric water vapor and water features in the spectrum B are caused by liquid water in the soil (Clark et al., 2002).

To investigate the effects of AC methods as one of the objectives of this study, I tested different atmospheric condition parameters that require user's selection. Levin (1999) states that the most important parameters of the atmosphere are the aerosol type, gases and water vapor amount that vary in space and time. The aerosol type represents a concentration of different aerosol types in the air. It includes absorption and scattering properties of the aerosols and their wavelength dependence properties. Water vapor

amount is the total amount of the gas in the atmospheric column from the ground to the top of the atmosphere, and it is measured as the mass of the water molecules in the atmospheric column over each square cm of the ground surface (Harris Geospatial Solutions, 2018a). In FLAASH, water vapor amount and aerosol type are set by the user. For multispectral sensors that do not have bands in water vapor absorption regions (9.2μm-9.6μm), a constant and standard atmospheric parameter is used for the water vapor. The water vapor amount is selected based on the surface temperature, the season of the year and latitude of the locations.

Regarding the aerosol type, FLAASH has several different aerosol models. In this research we used rural aerosol type. The rural aerosol model represents aerosols in continental areas and is assumed to be composed of 70% of water-soluble substance (ammonium, calcium sulphate and organic compounds) and 30% of dust like aerosol (Abreu et al., 1996). The urban model is the same as the rural aerosol type but with the addition of aerosols from combustion products and industrial sources. It is a mixture of 80% of rural type aerosols and 20% of soot-like aerosols (carbonaceous aerosols released from burning fossil fuels, coal, oil and gas) (Abreu et al., 1996), Since Kangankunde is located in continental areas and it is not close to industries, rural aerosol model was used in this study.

3.2.6. FLAASH-The Fast Line-of-sight Atmospheric Analysis of Spectral Hypercubes

FLAASH is commercially available as an add-on to the ENVI software, developed by Spectral Sciences, Inc. and the Air Force Research Laboratory (Anderson, 1999). It is based on MODTRAN-5 radiative transfer code and operates only in VNIR-SWIR regions up to 3.0μm not including the longwave infrared region. The basic principle of the FLAASH algorithm is described as below in short. FLAASH calculates image reflectance- ρ using the standard equation for spectral radiance at sensor L:

$$L = \left(\frac{A\rho}{1-\rho eS}\right) + \left(\frac{B\rho}{1-\rho eS}\right) + La \qquad (1)$$

where:

ρ is the pixel surface reflectance

ρe is an average surface reflectance for the pixel and a surrounding region

S is the spherical albedo of the atmosphere

La is the radiance back scattered by the atmosphere

A and B are coefficients that depend on atmospheric and geometric conditions but not on the surface (Perkins, 2005).

Each of these variables depends on the spectral channel; the wavelength index has been omitted for simplicity. The first term in Equation (1) corresponds to radiance that is reflected from the surface and travels directly into the sensor, while the second term corresponds to radiance from the surface that is scattered by the atmosphere into the sensor. The distinction between ρ and ρe accounts for the adjacency effect (spatial mixing of radiance among nearby pixels) caused by atmospheric scattering ((Perkins et al., 2005). To ignore the adjacency effect correction, set ρe=ρ. However, this correction can result in significant reflectance errors at short wavelengths, especially under hazy conditions and when strong contrasts occur among the materials in the scene.

The values of A, B, S and La are determined from MODTRAN calculations that use the viewing and solar angles and the mean surface elevation of the measurement, and they assume a certain model atmosphere, aerosol type, and visible range. The values of A, B, S and La are strongly dependent on the water vapor column amount, which is generally not well known and may vary across the scene. To account for unknown and variable column water vapor, the MODTRAN calculations are looped over a series of different column amounts, then selected wavelength channels of the image are analyzed to retrieve an estimated amount for each pixel. Specifically, radiance averages are gathered for two sets of channels: an absorption set centered at a water band (typically 1130 nm) and a reference set of channels taken from just outside the band. A lookup table for retrieving the water vapor from these radiances is constructed.

3.2.6.1. Data preparation for FLAASH

FLAASH uses the calibrated radiance data in a floating-point, long integer (4-byte signed), or integer (2-byte signed or unsigned) data type, and the interleave must be BIL or BIP. The ASTER image from 22 October 2004 was provided in TIFF format with the unsigned integer data type. First, VNIR and SWIR images were stacked together, and here, VNIR data was resampled to a 30m resolution of SWIR data pixel size to preserve the original spatial and spectral information of the SWIR bands of ASTER. Because the SWIR bands contain the diagnostic spectral features of the alteration minerals and later, the mineral mapping will be performed based on these bands. This combined data was then transferred into calibrated radiance data using ENVI's 'Radiometric Calibration' tool with a scale factor of 0.1. FLAASH requires input image to be in floating-point data type in units of [μW/ (cm² * sr * nm)]. This scale factor 0.1 converts radiance values from the units of [W/ (m² * sr * μm)] into units of [μW/ (cm² * sr * nm)].

3.2.6.2. Input parameters required for FLAASH

Scene and sensor information including the scene center location, the sensor type, altitude and flight date and time were all filled based on the information in the header file of the image, except the ground elevation value. This value was set to 0.793km according to the average elevation retrieved from DEM of the Kangankunde hills.

Regarding the atmospheric condition parameters, first, an atmospheric model must be selected by the user from one of the standard atmosphere models according to their water vapor amount. In case of absence of this information, the atmosphere can be selected based on surface air temperature of the area or based on a seasonal-latitude surface temperature model table provided by FLAASH (Harris Geospatial Solutions, 2018a).

Next, an aerosol model of the atmosphere was selected. As stated earlier, this study used rural aerosol model rural. The visibility was set to 40km according to the weather condition of the day of ASTER image acquisition- cloud-free and clear skies.

Besides the main input parameters required in the FLAASH, a 'Multispectral setting' is provided for multispectral sensors to retrieve the water vapor and aerosol amount based on the input image. Regarding the aerosol retrieval, the combined VNIR and SWIR ASTER image allowed to perform aerosol retrieval function using the bands at 0.6610μm and 2.1670μm, which are band 2 and band 5 of ASTER image respectively.

Table 3. The input parameters used in FLAASH for the ASTER image.

Scene and sensor parameters	Value
Sensor Type	ASTER
Sensor altitude (km)	705
Scene center location (LatLon)	(-14.8511428177241, 34.701242)
Flight date	22 OCT 2004
Flight time (GMT)	07:58:28
Pixel size (m)	30
Ground elevation (km)	0.793
Atmospheric parameters	
Atmospheric model	Tropical
Aerosol model	Rural
Initial visibility	40
Multispectral settings	
KT upper channel	ASTER-band5(2.1670)
KT lower channel	ASTER-band2(0.6610)
Max.upper.chan.reflectance	0.1
Reflectance ratio	0.45

3.2.6.3. Image processing in FLAASH

After entering all the required input parameters, FLAASH was run. It was then observed that the reflectance values obtained were much higher beyond the limit and some were in negative values, to remove this anomaly, an equation called Post FLAASH band processing equation was applied which is given by:

(B1 le 0)*0+(B1 ge 10000)*1+(B1 gt 0 and B1 lt 10000)*float (b1)/10000 (2)

The figure 5 below show band statistics before and after applying Post FLAASH processing equation.

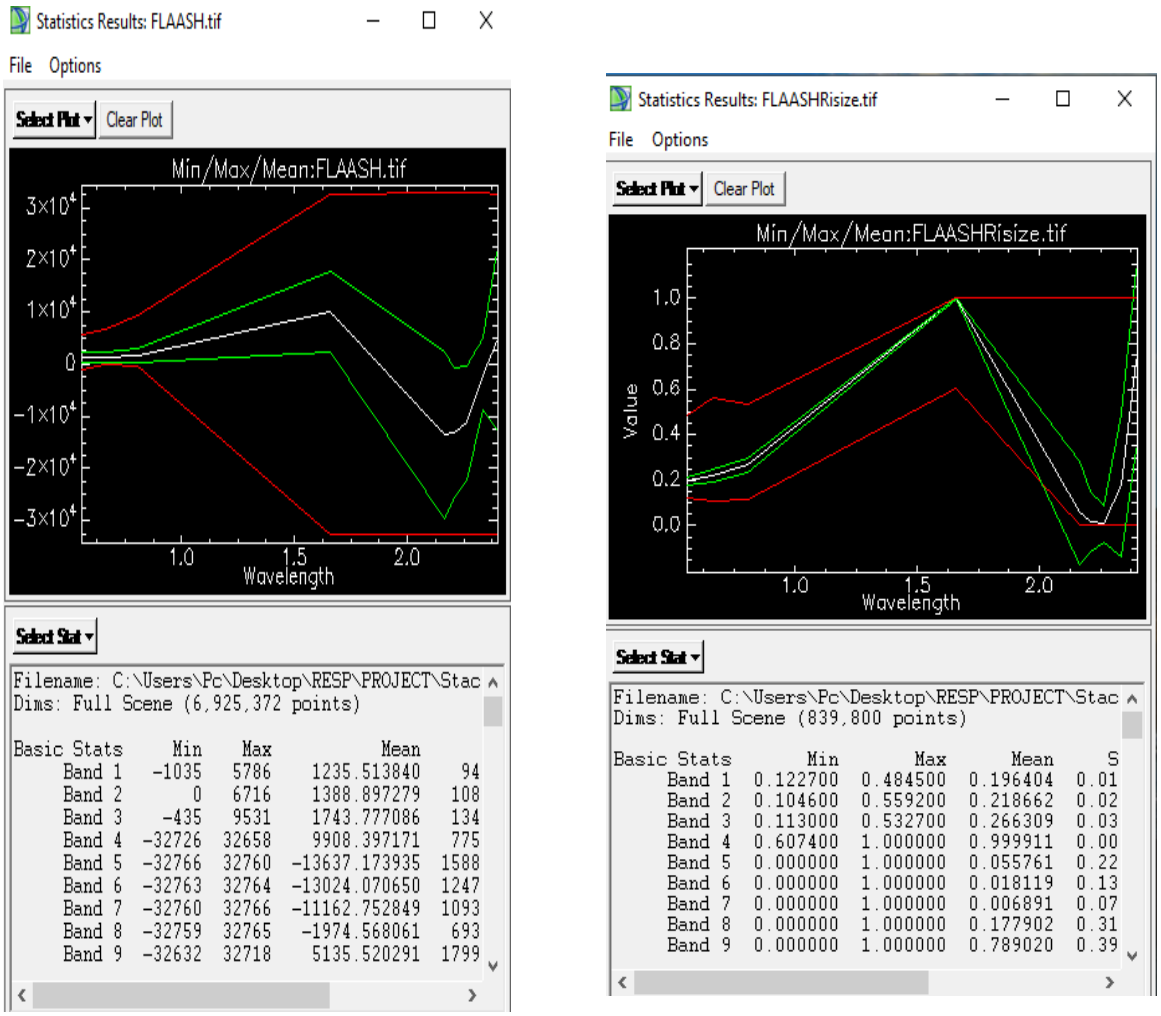


Figure 5. Showing statistical results before and after applying post FLAASH processing equation

3.2.7. Log Residuals

The log residuals method produces a pseudo reflectance dataset by dividing each pixel's spectrum by the spectral geometric mean and the spatial geometric mean. No user input is required to run this method. The algorithm residuals of dataset are defined as the input spectrum divided spectral geometric mean, then divided by spatial geometric mean (Green & Craig, 1985). The geometric mean is used because the transmittance and other effects are considered multiplicative. The spectral mean is the mean of all bands for each pixel and removes topographic effects. The spatial mean is the mean of all pixels for each band accounts for solar irradiance, atmospheric transmittance and instrumental gain.
Log residuals correction is similar to IARR (Internal Average Relative Reflectance) in that both tools use only in-scene statistics to produce results (Harris geospatial, 2018).

3.2.7.1. Image Processing with Log Residuals

As stated above, log residual method does not require user input. As such, the method was selected and stacked bands were chosen and run to produce the output image file.

3.2.8. Comparisons of atmospheric correction results

3.2.8.1. Qualitative visual comparison of reflectance spectra

Evaluation of atmospheric correction method's capability to recover surface reflectance is commonly performed on a qualitative basis, rather than quantitative, using the visual comparison of corrected image and field or library data on limited target areas (Ben-Dor et al., 2004).

Two areas were selected from the image from which reflectance spectra were derived for both two corrected images. Then the extracted image spectra from the outcomes of both atmospheric correction methods were directly compared and then plotted together with library data spectra for visual comparison.

3.2.8.2. Quantitative comparison and analysis

Apart from the visual and qualitative comparisons of absolute reflectance values, we did a quantitative spectral similarity comparison between the image and the field spectra. For the comparison, we used the Spectral Analyst tool in ENVI software. This tool uses SAM-Spectral Angle Mapper and SFF- Spectral Feature Fitting methods to score the match of a target spectrum to a reference spectrum (Harris Geospatial Solutions, 2018b). In SAM method, the target reflectance spectra (the image spectra) are compared to the reference spectra (the corresponding field spectra) looking for angular similarity between the two spectra (Asadzadeh et al., 2016). The spectra with a lowest angular difference with reference spectra gain the highest score, thus indicating the closest match. The method SFF is an absorption feature based method which compares the image spectra with reference spectra to fit using a least-square technique (Harris Geospatial Solutions, 2018b).

3.2.9. Mineral mapping

To evaluate differences in the mineral group maps produced from the output of AC methods, the satellite images were analyzed by using band ratio as mineral mapping technique to extract alteration minerals at Kangankunde area. The satellite images used in this analysis were the FLAASH corrected images and log residual corrected images. I used three sets of band ratios.

In this research, I used ASTER band calculation algorithm defined by Rowan (Aleks & Oliver, 2004). The three ASTER band ratios were selected based on the targeting mineral groups which are; 1. Al-OH, 2. Mg-OH, and 3. Fe-OH. The table 4 below summarizes the ASTER bands in the SWIR region and used band ratio algorithms. The resulting band ratio images were compared visually.

3.2.9.1. Band ratio techniques

Band Ratios are used to enhance the spectral differences between bands and to reduce the effects of topography (Sabins, 1999). Dividing one spectral band by another produces an

image that provides relative band intensities. The image enhances the spectral differences between bands. For instance, when using ASTER data, the band 5/band 7 ratio can be calculated and be used to produce an enhanced image (Abdeen et al., 2001). ENVI output band ratio images are either floating-point (decimal) format or byte data format. Floating-point format is the default. When using band ratios, specific bands were specified as numerator and denominator. The band ratio is the numerator divided by the denominator. ENVI checks for division-by-zero errors and sets them to 0. ENVI also allows to calculate multiple ratios and output them as multiple bands in one file. Figure 6 below, shows rock geochemistry at kangankunde which was used to determine the type of band ratios to use.

In this study, three sets of ASTER bands ratio calculation algorithm defined by Rowan (Aleks & Oliver, 2004) were used which are; Aluminium hydroxide band ratio (Al-OH), Iron-hydroxide band ratio (Fe-OH) and Magnesium hydroxide (Mg-OH) band ratio. Those three ASTER band ratios (relative band depth) were selected based on the targeting mineral groups which are: 1. Calcio-carbonatite, 2. Ferro-carbonatite, and 3. Magnesiocarbonatite.

The major- and trace-element compositions of the carbonatites are summarized in figure 6 (Chikanda et. al, 2019). These carbonatites use the molar proportions of CaO, MgO, and (FeO + MnO), the Kangankunde carbonatite are classified as magnesiocarbonatite and ferrocarbonatite (figure 6). Chikanda also noted that a larger group of the carbonatites are compositionally similar to dolomitic carbonatites, the presence of variable amounts of iron results in a compositional trend towards ankeritic carbonatites. Similar trends were observed for most Kangankunde carbonatite data studied by Broom-Fendley et al (2017).

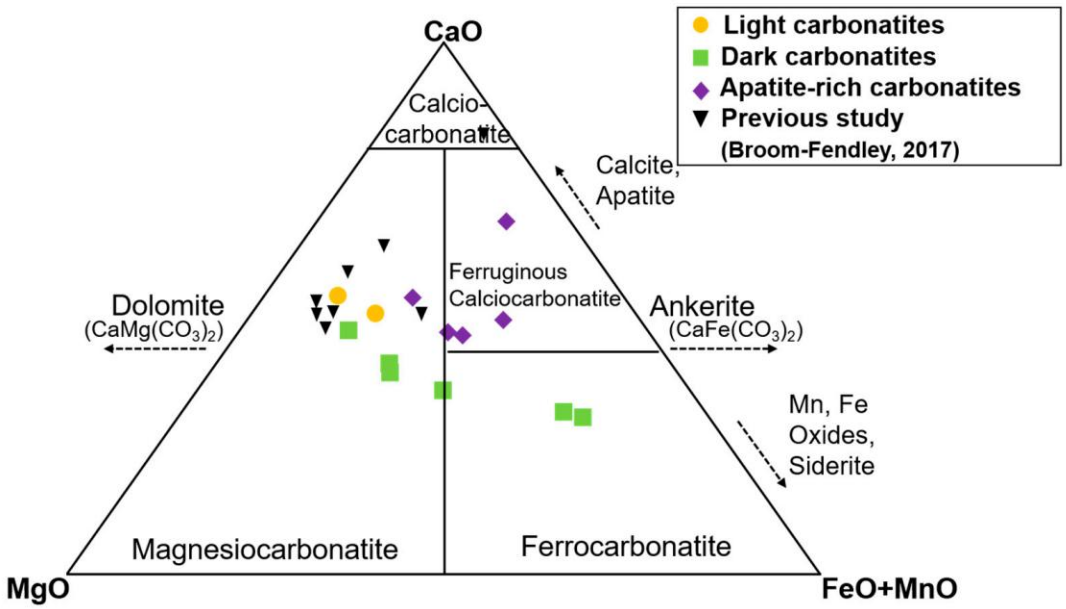


Figure 6. Classification of the Kangankunde carbonatites using molar proportions of CaO, MgO, and FeO + MnO (after Grittins and Harmer). Arrows indicate the trends that occur with increasing contents of the specified minerals.

3.2.9.1.1. Al-OH band ratio

To distinguish the occurrence of calcio-carbonatite mineral groups (Eq. 2), the band 5 and band 7 having high reflectance were added and their sum divided into band 6 with low reflectance.

$$\frac{(\mathbf{b5}+\mathbf{b7})}{\mathbf{b6}} \qquad (3)$$

In this band ratio method, calcio-carbonatite with large quantity of Al-OH minerals will appear as a bright pixel.

3.2.9.1.2. Fe-OH band ratio

This band ratio was used to characterize iron hydroxides mineral groups. the Fe-OH and CO_3 absorption features are located at the wavelength between 2.3μ to 2.5μm which coincide with band 7. Therefore, in this study bands 6 and 8 where there is high reflectance

of these minerals were added and their sum was divided by band 7 where there is absorption feature.

$$\frac{(\mathbf{b6+b8})}{\mathbf{b7}} \qquad (4)$$

3.2.9.1.3. Mg-OH band ratio

The Mg-OH absorption feature is situated in 2.30 to 2.35 μm equivalent with bands 8 of ASTER. To identify Mg-OH mineral groups (chlorite and calcite), this study used the (7 + 9)/8 band ratio.

$$\frac{(\mathbf{b7+b9})}{\mathbf{b8}} \qquad (5)$$

All those set of band ratios were computed using band math tool in ENVI to produce a single band image.

Table below summarizes the ASTER bands in the SWIR region and used band ratio algorithms. The resulting band ratio images and mineral index maps were compared visually.

Table 4. ASTER bands and band ratios by Rowan

Rowan's band ratios		
AlOH	(S5+S7)/S6	(b5+b7)/b6
MgOH	(S7+S9)/S8	(b7+b9)/b8
FeOH	(S6+S8)/S7	(b6+b8)/b7

4. Results and Discussion

4.1.1. FLAASH and Log residual corrected images

FLAASH and Log residual atmospheric correction methods were applied to the ASTER image with 9 bands in VNIR and SWIR wavelength regions. Two different aerosol models namely rural and urban were as well tested with the purpose of defining the optimal aerosol type for the study area Kangankunde. Other required input parameters and their selections have been explained in above chapters.

To compare reflectance spectra between the two AC methods and with library spectra, a region of interest (ROI) was created for the site P1. The mean spectra of the two sites were extracted from the statistics of ROI overlaid on FLAASH and Log residual corrected images. Figure 1 shows the radiance spectrum of site P1 before FLAASH and Log residual methods were applied on the image. The other subsequent figures show the reflectance spectra after FLAASH and Log residual methods were applied on the ASTER imagery.

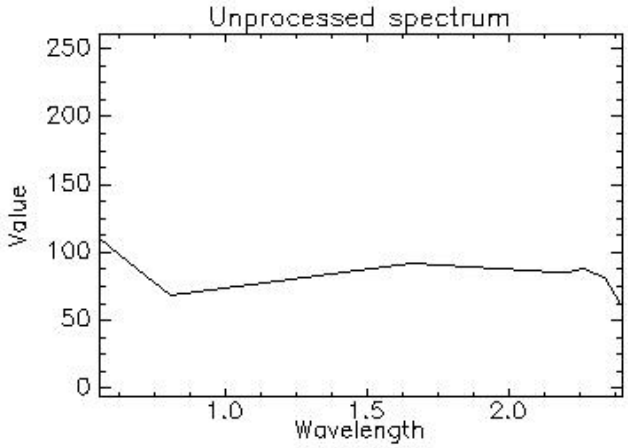


Figure 7. Showing spectrum for unprocessed ASTER data from one ROI image data.

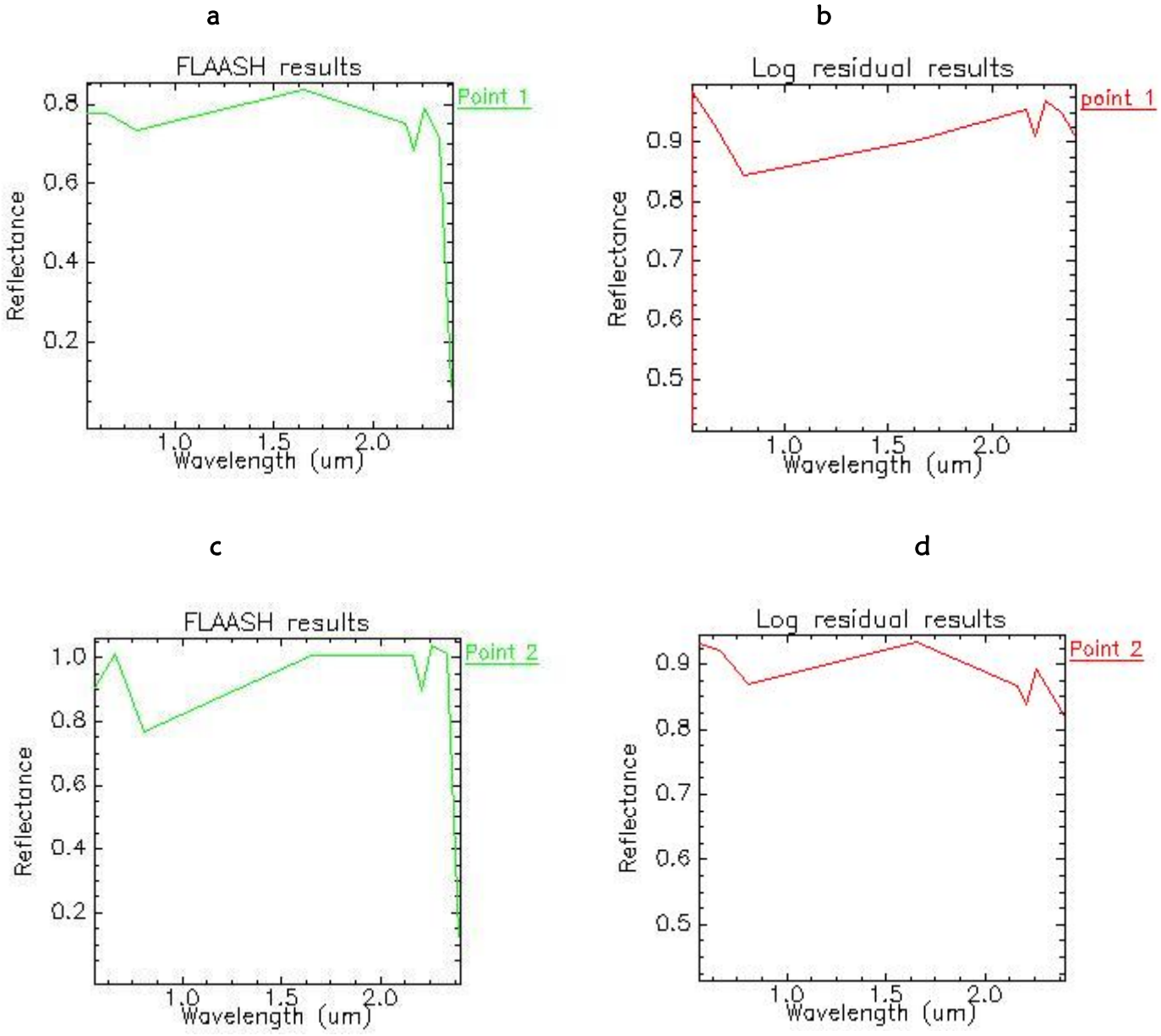


Figure 8. FLAASH and Log residual corrected image spectra of different sites.

Log residual results (**b** and **d**) show more variation for each reference site unlike the FLAASH results for the same sites. The value difference comprises 5% in the 2.21 um band. Thou in this band, FLAASH a deeper absorption feature than log residual.

4.1.2. Comparison of atmospheric correction results with ASTER USGS resampled library data

4.1.2.1. Comparison between FLAASH results USGS ASTER resampled library spectra

The mean reflectance spectra of the two reference sites extracted from FLAASH corrected images were directly compared and plotted together with the resampled field spectra (Figure 9).

There is reasonable conformity in shape between library and image spectra. For the both sites P1 and P2, the overall shape of the image spectra is similar to the field spectra within the standard deviation limits. Besides, an unknown minimum occurs at the 0.75μm, while it is not present in the library spectra. Regarding the wavelength 1.7μm, FLAASH overestimate reflectance on both sites than the library data with that in site P2 being much higher. In general, the image reflectance spectra are always higher than the library spectra for FLAASH results.

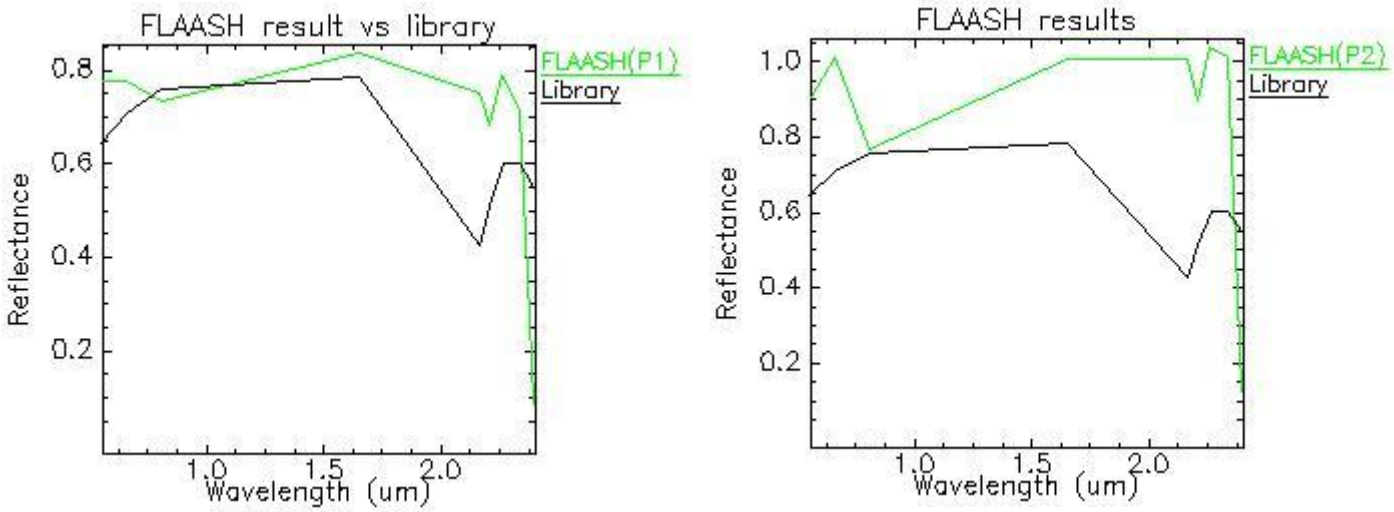


Figure 9. Comparison between library spectra and FLAASH corrected image spectra.

The image spectra of the site P1 show a good overall similarity in spectral shape with the USGS ASTER resampled spectra (Figure 9a). In contrast, on site P2 reflectance levels were higher than the library data across the wavelength.

4.1.2.2. Comparison between Log residual and USGS ASTER resampled library data

The mean reflectance spectra of reference sites extracted from Log residual corrected images were directly compared and plotted together with the ASTER resampled USGS library spectra (Figure 10).

Regarding the validation site P1, the image reflectance values are higher but not as much as those on site P2. Site P2 show much higher reflectance values with variations of about 14% when compared to library reflectance values. In terms of spectral shape, image spectra look overall similar with library spectra but with an absorption at wavelength 0.75μm of which library spectra show a peak. The site P2 (figure 10 b) show more similar overall shape than site P1.

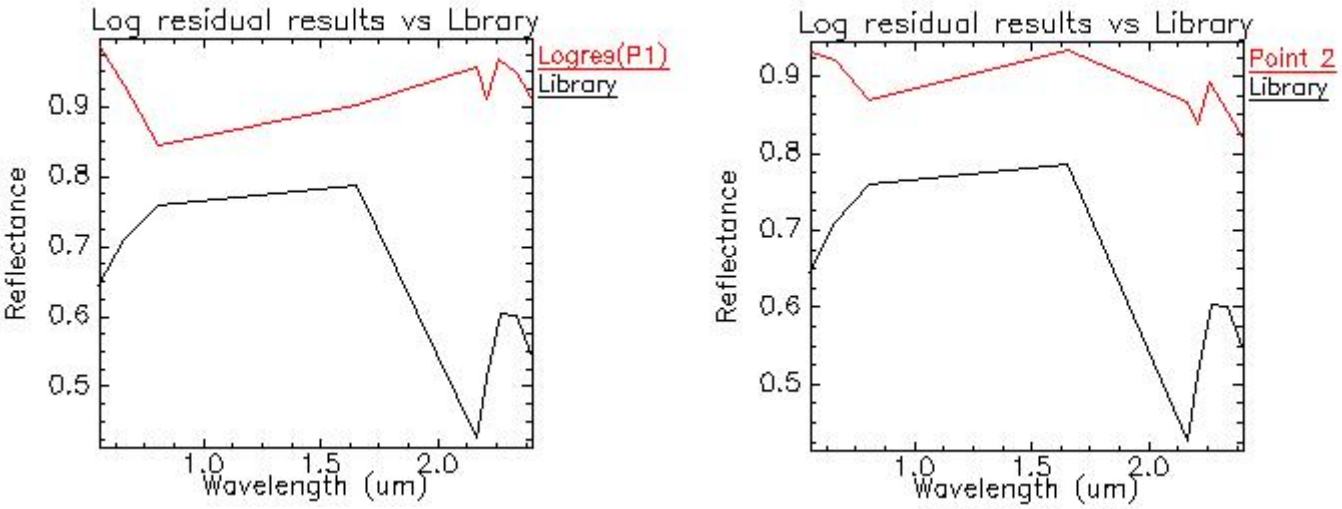


Figure 10. Comparison between resampled ASTER library spectra and Log residual corrected image spectra for the two sites P1 and P2.

4.1.2.3. Comparison between FLAASH, Log residual and library data

In the previous sections, outcomes of FLAASH and log residual atmospheric correction (AC) methods have been compared separately with the USGS ASTER resampled library reflectance spectra. This section we compare both two AC methods with library spectra by plotting them together.

Figure 10 displays comparative plots of the resampled ASTER library spectra and the image spectra corrected by Log residual and FLAASH for each of two selected sites. Visually, the overall shape of the FLAASH corrected image spectra are more similar to the library spectra than log residual results. Log residual corrected image spectra produces a shallow absorption feature at wavelength 2.21μm as compared to FLAASH corrected image and library reflectance spectra which shows deeper absorption feature. Visually, FLAASH produced a much similar reflectance spectra to that of library spectra data.

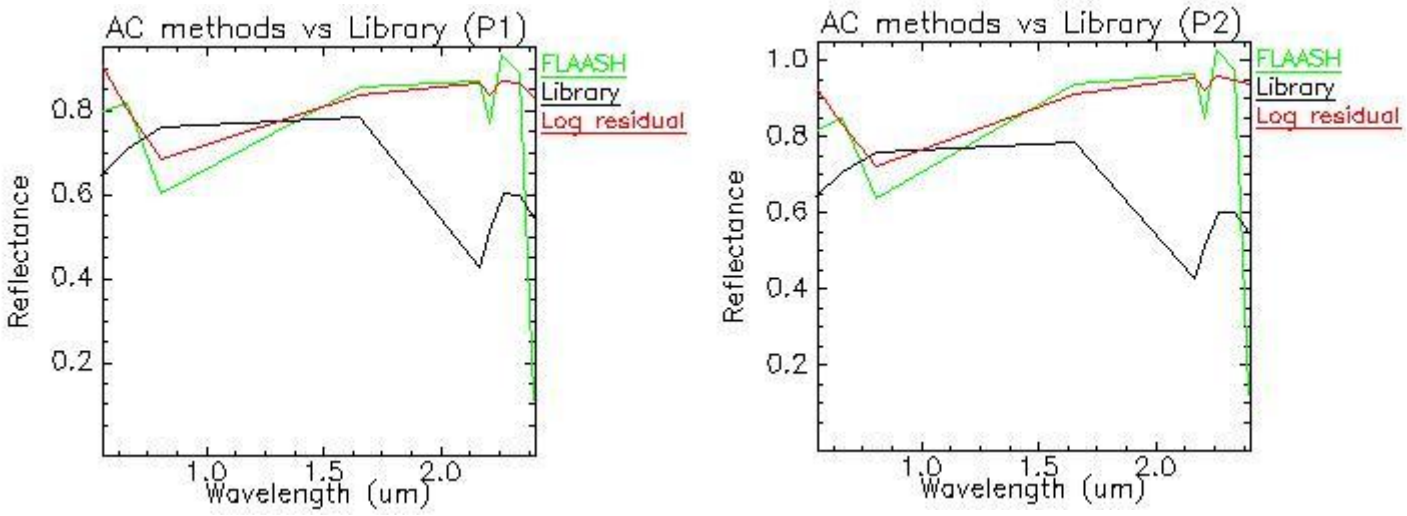


Figure 11. Spectral comparison between Log residual, FLAASH and the resampled ASTER library spectra of two different sites P1 and P2.

In terms of reflectance differences, both AC methods produced results of closer to the library data in the VNIR, where FLAASH AC produced a closest match of 1% at the

central wavelength 0.66μm at site P1 (Figure 12). The log residual's closest match was at site P1 but at the wavelength 1.65μm where the value was 2%. The log residual produced the most overestimated result with value of almost 51% at the wavelength 2.17μm. In general, the FLAASH atmospheric correction methods presented specific absorption features very well such as at the wavelength 2.21μm, the depth of absorption feature was very high unlike the log residual results which made the FLAASH results to be in closer match to the library data at this point.

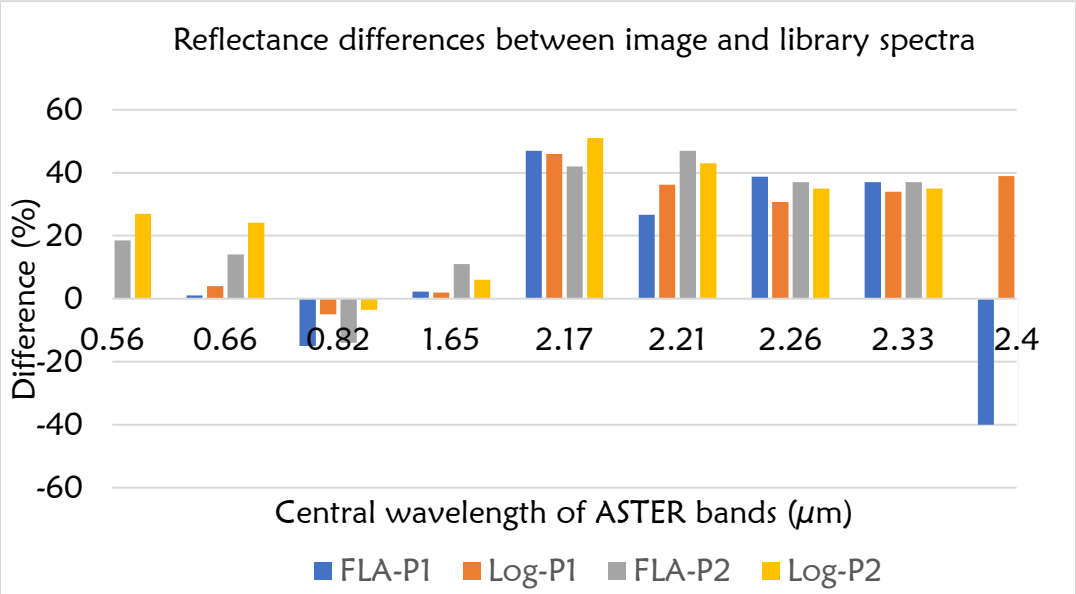


Figure 12. Differences of the surface reflectance estimated by FLAASH (FLA) and Log residual (Log) and USGS ASTER resampled library spectra data. Positive values show overestimation and negative values show underestimation of the reflectance compared to the library data.

The two AC image spectra were then compared with library USGS ASTER resampled spectra data using two spectral matching techniques SAM and SFF (Table 5). From both SAM and log residual, FLAASH AC spectra got the highest scores in both sites P1 and P2. This implies that the FLAASH spectra was in close match to library spectra. The log residual spectra got the least match in both sites. The FLAASH spectra got the its highest score at

site P2 in both techniques though the SAM technique produced the highest score. The log residual result got it least score at the site p2 with SFF technique indicating worst match.

Table 5. Spectral similarity results between AC corrected image spectra and library spectra using SFF and SAM methods.

site	FLAASH		Log residual	
	SFF	SAM	SFF	SAM
P1	0.437	0.551	0.413	0.511
P2	0.452	0.566	0.428	0.523

4.1.3. Mineral mapping results

After direct comparisons of reflectance spectra of two scenes and different atmospheric correction (AC) methods, the FLAASH corrected image and Log residual reflectance image were analyzed using band ratio techniques to extract alteration minerals groups at Kangankunde. These analysis aims to evaluate differences in mineral maps produced from above mentioned two different reflectance images. The comparisons of the band ratio results were done visually.

4.1.3.1. Band ratio results

Three mineral indices developed by Rowan (Aleks & Oliver, 2004) for ASTER data, were applied to the ASTER image. The bands used in mineral indices and their wavelengths are shown below. Al-OH indices was chosen aiming to map feldspar breccia group of minerals at the study area. On the other hand, Mg-OH band ratio was used to map minerals such as Dolomite carbonatite on the study area, Fe-OH band ratio was used to map ferrous carbonate group at the study area. The used band ratios are:

1. Mg-OH: (S7+S9)/S8
2. Al-OH: (S5+S7)/S6
3. Fe-OH: (S6+S8)/S7

Figures 12 and 13 below, shows the results of band ratios. The Al-OH band ratio images showed similar overall pattern in both two corrected images but FLAASH corrected images showed more information in the lower right half of the image. The Mg-OH band ratio images also showed similar pattern throughout. The Fe-OH band ratio is the one which showed more differences as the FLAASH corrected image showed more enhanced Fe-OH mineral groups than the Log residual images. The area also seems to have less Fe-OH mineral groups when related to the other two groups explained above. Differences in value ranges were also low. Regarding the Al-OH ratio images, data range of log residual image was the highest and consequently, produced relatively intense map in the lower left corner compared to the FLAASH.

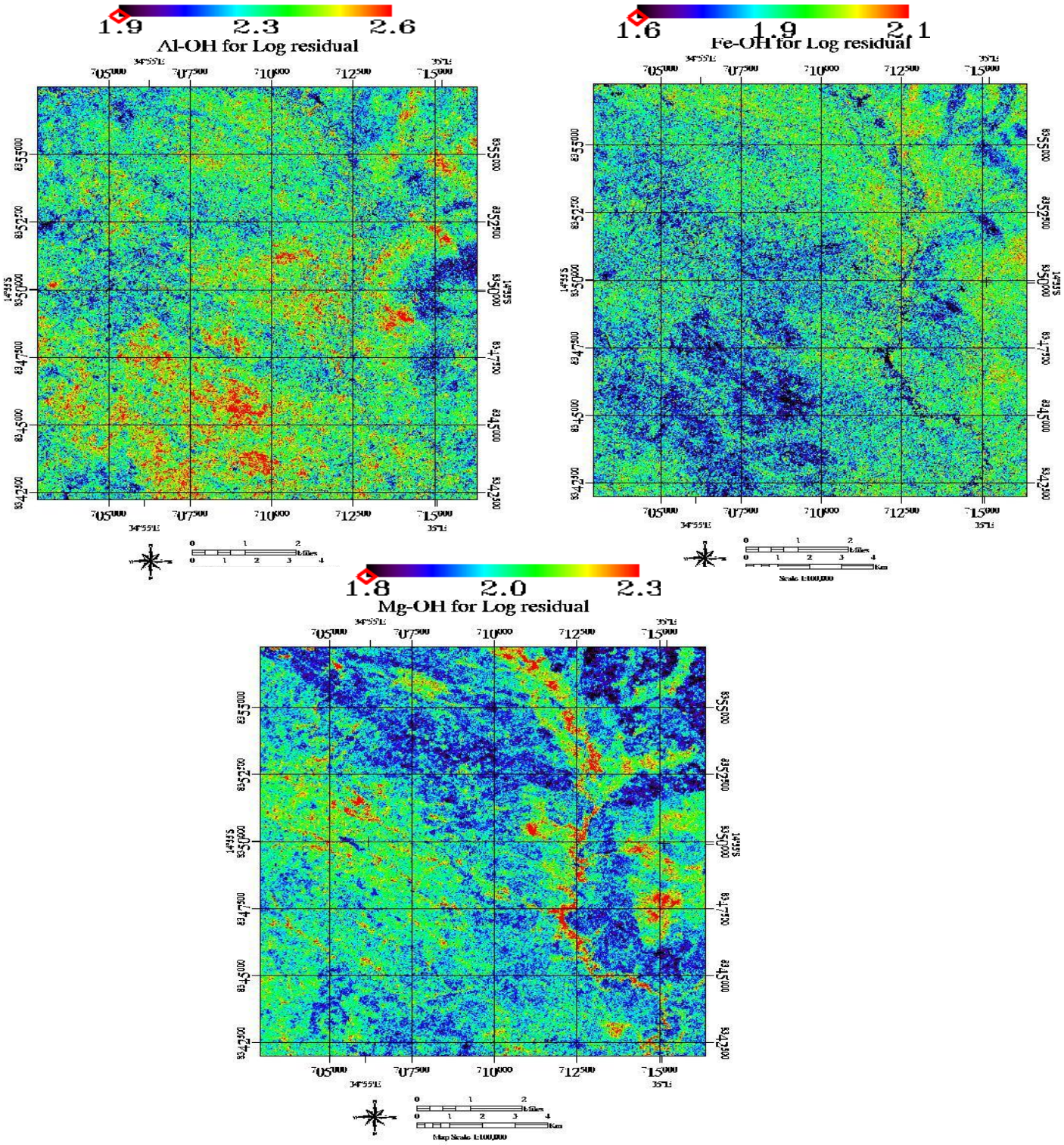


Figure 13. Band ratio mineral group maps for Log residual.

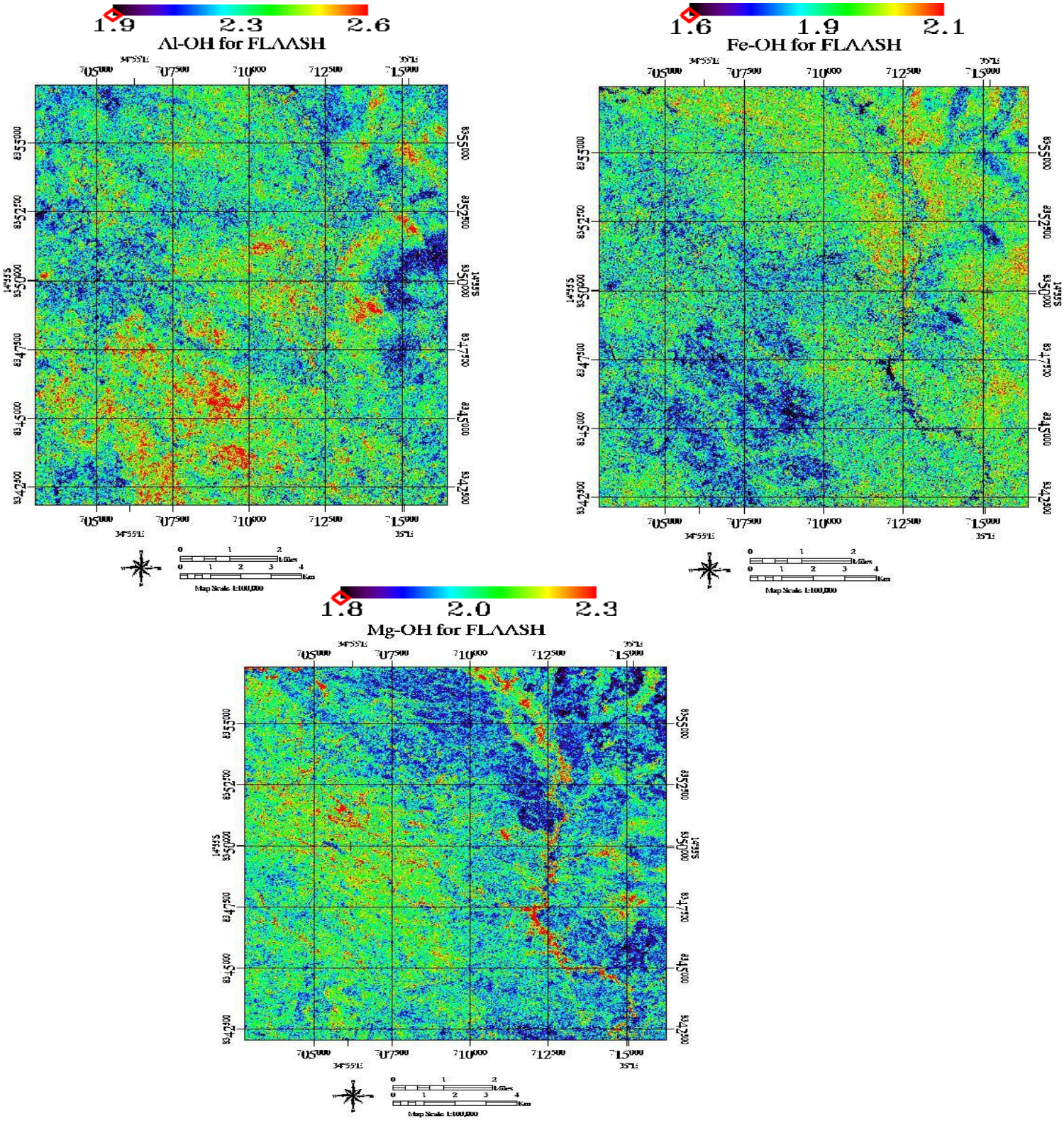


Figure 14. Band ratio mineral group maps for FLAASH.

Band ratios produced from each AC method, were used to generate RGB images for each AC method as shown in figure 14 below. The results indicate that Mg-OH and Al-OH mineral groups at Kangankunde are spectrally strong, while the Fe-OH mineral group has moderate contribution. Visually, FLAASH RGB map showed more Fe-OH mineral group unlike how they are represented in the log residual. The log residual result show some more unidentified pixels in blue, while FLAASH results show almost good distinction of each mineral group and the areas which are dominated by one group can easily be differentiated from the others.

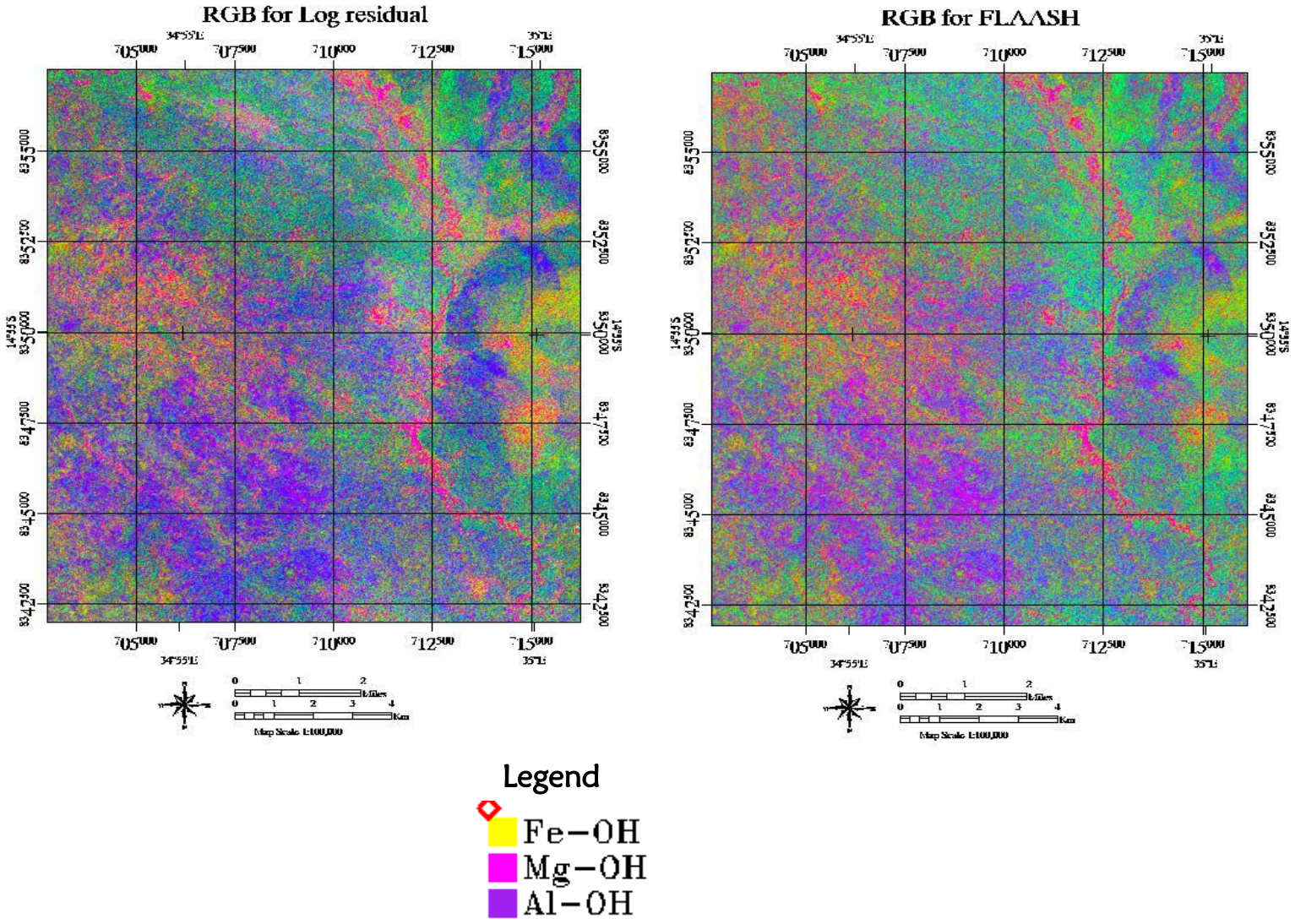


Figure 15. RGB maps for Log residual and FLAASH produced from Mg-OH, Fe-OH and Al-OH band ratios.

4.2. Discussion

In this research, two different radiative transfer models (RTM) based atmospheric correction (AC) methods Log residual and FLAASH were applied to ASTER image acquired on 22 October 2004. Their results were directly compared with USGS ASTER resampled library data. comparisons were also made between those two AC methods. Finally, band ratio technique was used for mapping mineral groups at kangankunde. The following subsections will discuss the results comparisons of AC methods and mineral mapping results, and the side issues faced during the research.

4.2.1. Comparisons of atmospheric correction results with library data

Spectral comparison of Log residual results versus the resampled USGS ASTER spectra data is presented in Figure 11. Overall, the reference sites' image spectra look relatively similar with library resampled spectra but the image spectra have higher reflectance values than library spectra almost across all wavelength. Also, in the wavelength of around 0.75μm there are some differences as the image spectra show an absorption feature while the library spectra show reflection. This difference may be caused by availability of some mixture in the pixel from where these spectra were extracted. However, this research did not focus on further investigations to confirm this assumption.

FLAASH produced the closer results to the library data for both sites P1 and P2. The FLAASH result showed a stronger absorption feature in the 2.21μm wavelength, whereas the log residual showed a shallow absorption feature and the library spectra showed the biggest absorption feature. This band at 2.21um is important for mapping Al-OH group of minerals as this is where this absorption feature is located.

For conclusion and ease of explanation, the results of FLAASH and Log residual methods were plotted together with the ASTER USGS resampled library spectra in figure 10. All in all, the FLAASH atmospheric correction method was found to produce the closer results to the library spectra than Log residual.

4.2.2. Mineral mapping results

The final objective of this research was to evaluate differences in mineral maps due to applying different atmospheric correction methods. For this purpose, the Log residual and FLAASH corrected images were analyzed by using band ratio techniques to map mineral groups at Kangankunde.

4.2.2.1. Band ratio results

Three band ratios by Rowan (Aleks & Oliver, 2004) for ASTER bands (see Table 4) were used to map different mineral groups such as Al-OH, Fe-OH and Mg-OH groups in the study area. Before processing the images, the vegetation effect was suppressed by masking pixels with NDVI values less than 0 and greater than 0.4 based on the vegetation analysis by Usman (2018). The comparisons of the band ratio products were done visually.

Generally, both corrected images show similar results. Though the FLAASH RGB image show more enhanced outputs than Log residual RGB image. On each individual band ratio images, the Al-OH band ratio produced a lot of such mineral groups which indicate that the area has a lot of Al-OH minerals than other minerals. This was more observed in FLAASH corrected images. The Fe-OH band ratio produced least results in both corrected images, but the FLAASH corrected image produced more enhanced Fe-OH mineral groups than Log residual corrected image.

Conclusions and Recommendations

This research aimed to determine the most suitable atmospheric correction method for ASTER satellite image. This study involved two methods which are FLAASH and Log residual methods applied on ASTER image. This ASTER image was acquired in October 2004 over Kangankunde in Balaka district of Malawi. The month of October was chosen as it appeared to be the best month of that year for remote sensing purposes after analyzing weather pattern for Balaka district. Kangankunde was chosen as it hosts different mineral groups that consist of VNIR and SWIR active minerals, this study also sought to know

whether different atmospheric corrections can influence mineral mapping results. Our results of AC comparisons and mineral mapping lead to the following conclusions:

- Our results showed that the reflectance image spectra of the reference sites did exhibit unknown features that are not present in the library spectra. These unknown features were present at the wavelength 0.75μm, hence there is need to inspect further.

- During the study, it is proposed to compare and evaluate then success of the two different atmospheric corrections for ASTER data beyond the scope of mineralogical mapping. All algorithms are compared with two different approaches; one with individual absorption features and with mineral mapping using band ratios. As a result of the study, all the atmospheric correction methods applied on the data are found to be successful in overall evaluation but with compromises varying in different wavelength regions. Despite the compromises in different wavelength regions FLAASH is found to be a better corrector algorithm for mineralogical mapping needs.

To summarize, through comparison of library data and atmospherically corrected image spectra acquired over Kangankunde, the study found that FLAASH method provides an efficient method for mineral exploration and geologic mapping of different mineral groups in general using ASTER imagery. However, it should be noted that during this study as discussed earlier, we encountered a number of problems and consequences that made AC comparisons complicated. Some of these problems are less spectral resolution of the ASTER sensor, there was no field data to make further comparisons such as producing scatterplots to see correlation between corrected images bands and the field spectra bands.

References

A. Kerr, H. Rafuse, G. Sparkes, J. Hinchey, & H. Sandeman. (2011). "Visible/infrared spectroscopy (VIRS) as a research tool in economic geology: background and pilot studies from Newfoundland and Labrador," Geological Survey, Report, vol. 11, pp. 145-166.

Abdeen, M.M., Allison, T.K., Abdelsalam, M.G., & Stern, R.J. (2001). Application of ASTER band ratio images for geological mapping in arid regions; the Neoproterozoic Allaqi Suture, Egypt. Geological society of America, 3, 289.

Abrams, M., Hook, S., & Ramachandran, B. (2004). ASTER Users Guide V2. NASA JPL. Retrieved from https://asterweb.jpl.nasa.gov/content.

Ben-Dor, E., Kindel, B., & Goetz, A. F. H. (2004). Quality assessment of several methods to recover surface reflectance using synthetic imaging spectroscopy data. Remote Sensing of Environment, 90(3), 389–404. https://doi.org/10.1016/j.rse.2004.01.014.

Broom-Fendley, S., Wall, F., Spiro, B., & Ullmann, C.V. (2017). Deducing the source and composition of rare earth mineralising fluids in carbonatites: Insights from isotopic (C, O,87Sr/86Sr) data from Kangankunde, Malawi. Contrib. Mineral. Petrol. 172, 96.

Chikanda, F., Otake, T., Ohtomo, Y., Ito, A., Yokoyama, T.D., & Sato, T. (2019). Magmatic-Hydrothermal Processes Associated with Rare Earth Element Enrichment in the Kangankunde Carbonatite Complex, Malawi.

Clark, R. N., Swayze, G. A., Livo, K. E., Kokaly, R. F., King, T. V. V., Dalton, J. B., & McDougal, R. R. (2002). Surface reflectance calibration of terrestrial imaging spectroscopy data: A tutorial using AVIRIS. In Proceedings of the 10th Airborne Earth Science Workshop. JPL Publication 02-1. Retrieved from ftp://popo.jpl.nasa.gov/pub/docs/workshops/02_docs/2002_Clark_web.pdf.

E.V.I. Solutions. (2014). Exelis ENVI online manual. Available: http://www.exelisvis.com/docs/home.html.

Gao, B.C., & Davis, C. O. (1997). Development of a line-by-line-based atmosphere removal algorithm for airborne and spaceborne imaging spectrometers. Proceedings of the Society of Photo-Optical Instrumentation Engineers (SPIE), 3118 (1997), 132–141. https://doi.org/10.1117/12.283822.

Green, A.A., & Craig, M.D. (1985). Analysis of aircraft spectrometer data, with logarithmic residuals, Proceedings of the Airborne Imaging Spectrometer Data Analysis Workshop.G. Vane and A. Goetz editors, JPL, pp111-119.

Gupta, R. P. (2018). Remote Sensing Geology (3rd ed.). Berlin: Springer Berlin Heidelberg. https://doi.org/10.1007/978-3-662-55876-8.

Kale, K. V., Solankar, M. M., Nalawade, D. B., Dhumal, R. K., & Gite, H. R. (2017). A Research review on hyperspectral data processing and analysis algorithms. Proceedings of the National Academy of Sciences, India Section A: Physical Sciences, 87(4), 541–555. https://doi.org/10.1007/s40010-017-0433-y.

Kokaly, R.F. (2011). PRISM: Processing routines in IDL for spectroscopic measurements (installation manual and user's guide, version 1.0)," US Geological Survey 2331-1258.

Kruse, F. A., Lefkoff, A. B., Boardman, J. B., Heidebrecht, K. B., Shapiro, A. T., Barloon, P. J., & Goetz, A. F. H. (1993). The Spectral Image Processing System (SIPS) - Interactive Visualization and Analysis of Imaging spectrometer Data. Remote Sensing of the Environment, v. 44, p. 145 – 163.

Kujjo, C. P. (2010). Application of remote sensing for gold exploration in the Nuba Mountains, Sudan (PhD thesis). Bowling Green State University.

Levin, N. (1999). Fundamentals of Remote Sensing. Trieste: Iternational Maritime Academy.

Liang, S., & Wang, J. (Eds). (2020). Advanced Remote Sensing: Terrestrial Information Extraction and Application (2nd ed.). Cambridge: Elsevier.

Neave, D.A., Black, M., Riley, T.R, Gibson, S.A., Ferrier, G., & Wall, F (2016). On the feasibility of imaging carbonatite-hosted rare earth element (REE) deposits using remote sensing.

Nikolakopoulos, K.G.; Vaiopoulos, D.A., & Skianis, G.A., (2002). A Comparative Study of Different Atmospheric Correction Algorithms Over an area with Complex Geomorphology in Western Peloponnese, Greece, Geoscience and Remote Sensing Symposium, IGARSS '02, IEEE International, 4, pp. 2492 –2494.

Perkins, T., Adler-Golden, S., Matthew, M., Berk, A., Anderson, G., Gardner, J., & Felde, G. (2005). Retrieval of atmospheric properties from hyper and multispectral imagery with the FLAASH atmospheric correction algorithm. In Schäfer, k., Comerón, A., Slusser, J.R., Picard, R.H., Carleer, M.R & Sifakis, N.I (Eds.) (p. 59790E). https://doi.org/10.1117/12.626526.

Qu, Z., Kindel, B. C., & Goetz, A. F. H. (2003). The high accuracy atmospheric correction for hyperspectral data (HATCH) model. IEEE Transactions on Geoscience and Remote Sensing, 41(6 PART I), 1223–1231. https://doi.org/10.1109/TGRS.2003.813125.

Richter, R., & Schläpfer, D. (2002). Geo-atmospheric processing of airborne imaging spectrometry data. Part 2: Atmospheric/topographic correction. International Journal of Remote Sensing, 23(13), 2631–2649. https://doi.org/10.1080/01431160110115834

Rowan, L.C., & Mars, J.C. (2003). Lithologic mapping in the Mountain Pass, California area using advanced spaceborne thermal emission and reflection radiometer (ASTER) data," Remote sensing of Environment, vol. 84, pp. 350-366.

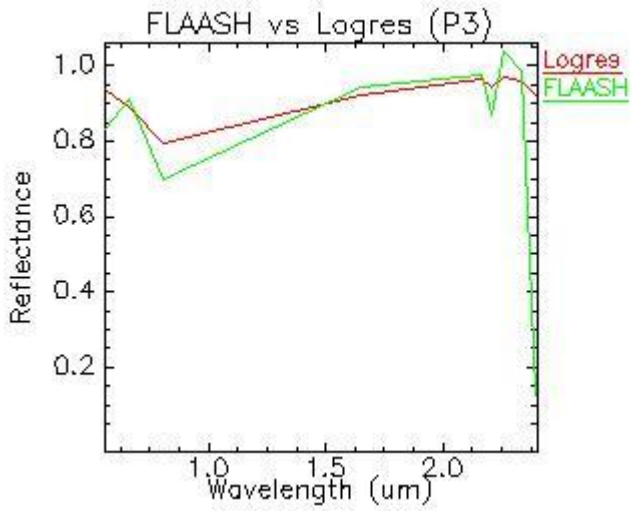
Tempfli, K., Kerle, N., Huurneman, G. C., & Jansen, L. L. F. (2009). Principles of Remote Horniman Sensing - An introductory text book (4th ed.). Enschede, The Netherlands: The International Institute for Geo-Information Science and Earth Observation (ITC).

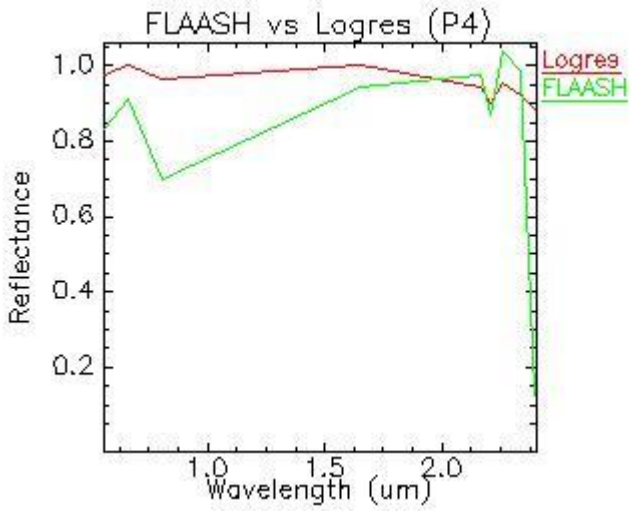
Vincent, R. K. (1997). Fundamentals of Geological and Environmental Remote Sensing. Prentice Hall, 370p.

Appendices

Appendix 2. FLAASH and Log residual results for the additional target areas.

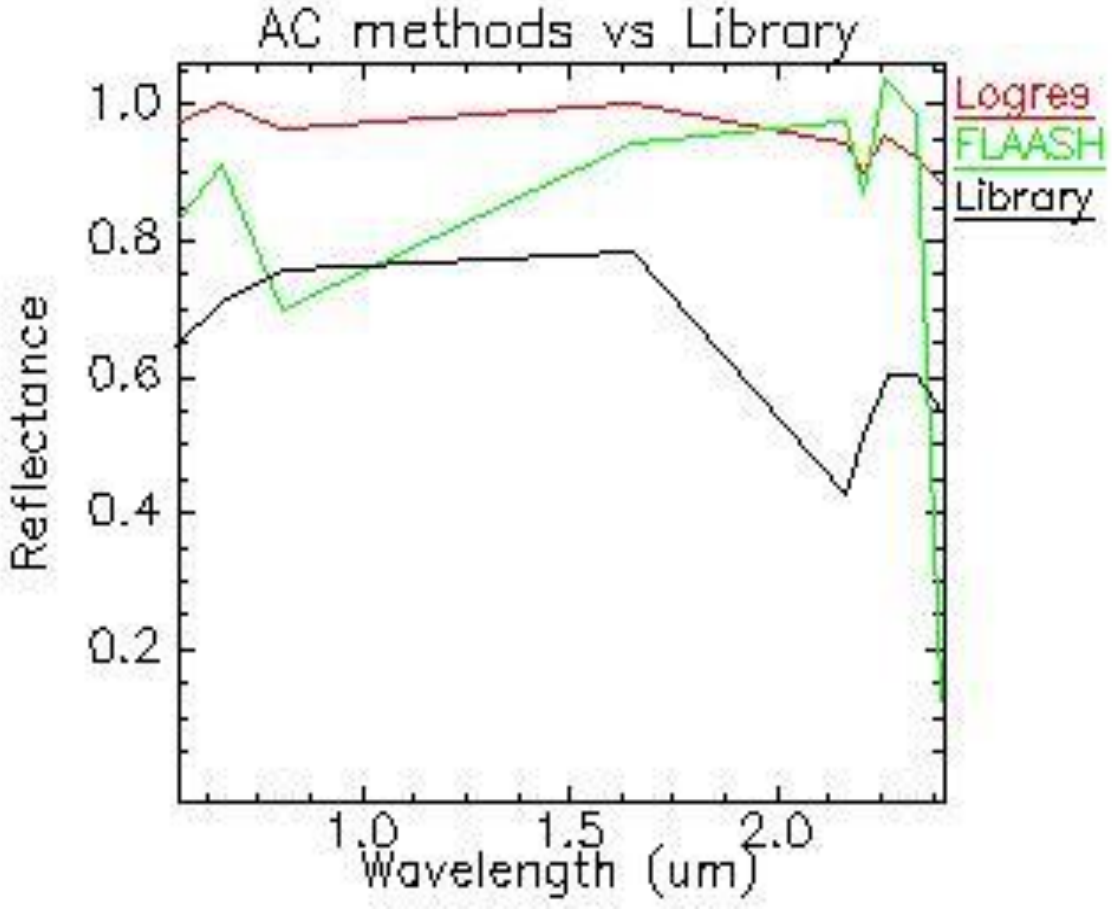
The surface reflectance spectra of the additional target areas collected from FLAASH and Log residual corrected images.





Appendix 2. Spectral comparison between FLAASH and Log residual results with library spectra.

The comparison is shown from P4 reference site.



Appendix 3. FLAASH input parameters description for different locations

FLAASH AC requires user input for different parameters based on the location where the image was captured and weather conditions of the area.

Model Atmosphere	Water Vapor (std atm-cm)	Water Vapor (g/cm2)	Surface Air Temperature
Sub-Arctic Winter (SAW)	518	0.42	-16° C (3° F)
Mid-Latitude Winter (MLW)	1060	0.85	-1° C (30° F)
U.S. Standard (US)	1762	1.42	15° C (59° F)
Sub-Arctic Summer (SAS)	2589	2.08	14° C (57° F)
Mid-Latitude Summer (MLS)	3636	2.92	21° C (70° F)
Tropical (T)	5119	4.11	27° C (80° F)

Appendix 4. Study area map

The map below shows the location of Kangankunde hills in Balaka district, Malawi

